Hardin, R., Beckermann, C., Foley, R., Griffin, J., and Poweleit, D., "Pressurized Steel Casting Trials," in Proceedings of the 78th SFSA Technical and Operating Conference, Paper No. 5.15, Steel Founders' Society of America, Chicago, IL, 2024.

Pressurized Steel Casting Trials

Richard Hardin and Christoph Beckermann, University of Iowa (UI)
Robin Foley and John Griffin, University of Alabama at Birmingham (UAB)
David Poweleit, Steel Founders' Society of America (SFSA)

Abstract

Recent casting trials were performed at Harrison Steel Castings Company (HS) and Waukesha Foundry to apply pressure to solidifying steel sand castings with an Automated Pressure Casting System (APCS) from Foundry Casting Systems (FCS). The trials investigated whether improved casting soundness and mechanical properties result from applying increased pressure during solidification. HS produced an 8630 platypus casting solidifying under atmospheric pressure and another under 10 atmospheres of pressure. HS also produced an 8630 wedge casting with both pressure conditions. Waukesha Foundry produced CF3 and CF3M plate castings likewise using both atmospheric and pressurized solidification conditions for both alloys. Pressure was ramped up to 10 atm as soon as the APCS was closed to promote the maximum effect on the casting system. Castings were radiographed, sectioned for tensile testing, and analyzed for fracture surface conditions. Surface gas porosity was not observed in the pressurized platypus casting; however, similar shrink porosity was found for both castings. Differences in dimensions were seen between the platypus castings. Simulation results showed feeding flow to the region with shrink was cut-off in the platypus castings. No difference reduction in shrink was observed since with pressure feeding flow was extended only by 1 minute. Applying pressure does not replace good foundry engineering practice, and a casting solidifying under pressure needs to be rigged to consider increased feeder demands. The platypus tensile specimens overall showed little difference in strength but, depending on location, some increase in ductility when pressurized. The difference is likely due to reduced microporosity and its location dependency since only some regions received a benefit from pressure. The wedge and the plate castings both solidify directionally, and macro shrinkage was not expected even in the non-pressurized castings. For the plates and wedges, edge tensile specimens showed little difference, and any small difference is likely due to a heat treatment section size effect. Given that CF grades are highly ductile, no significant differences in mechanical properties from pressure was expected, as was observed. The trials did not yield evidence that pressure casting steel is beneficial to tensile properties, except for ductility at some locations. The trial demonstrated a benefit from increased feeding which could be exploited to increase yield. With rigging designed to take advantage of improved feeding, a pressure cast part could have reduced shrink and improved properties.

1. Introduction

The application of increased force on liquid feed metal during solidification assists feeding and reduces porosity in castings. The force on the liquid feed metal can be increased using centrifugal acceleration and by applying pressure during solidification. There is ample evidence in the literature dating back to the 1940's [1] that casting under increased pressure can provide improvements in feeding distances. UAB research for GM decades ago demonstrated a benefit in aluminum castings. Mercury Marine uses the Pechiney process to manufacture aluminum castings. UI research demonstrated capability of [2]. Hitchiner uses a proprietary pressure casting process. And a multitude of other proprietary pressure casting processes exist. However, it is an open question whether applying pressure during casting can improve the performance of steel castings and their mechanical properties, and if the process could be done effectively in production. In addition to improving feeding, pressure and a nitrogen environment should increase the cooling rate. A higher cooling rate could provide a smaller grain structure and result in enhanced properties. FCS developed the APCS prototype for foundry trials (Figure 1). The equipment was used for an initial trial that was reported on at the 2023 T&O Conference [3]. Additional pressure cast trials were completed in 2024 at HS and Waukesha Foundry to continue to investigate the merits of applying pressure during solidification.

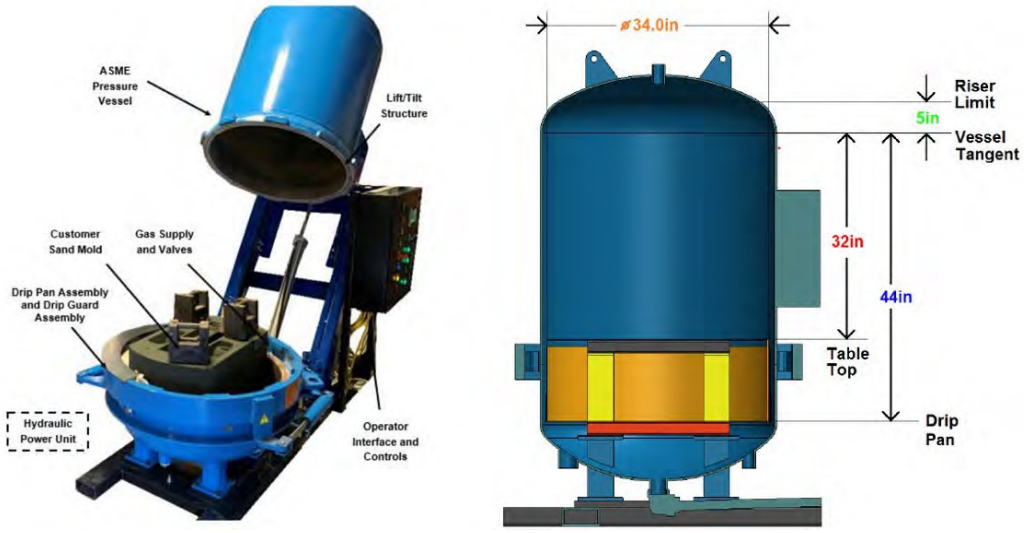

Figure 1: FCS Automated Pressure Casting System

Three parts were cast in the trials. HS made the "platypus" in an 8630-type grade, which has been used in recent SFSA process-driven performance modeling research and an 8630-type UAB wedge, which has been used in recent High Strength Steel research [4]. Waukesha Foundry made a 9"x9" (tapered 1" to 2" bottom to top) plate casting in both CF3 and CF3M. All four of these castings were made both under normal atmospheric pressure conditions and in the pressurized APCS. The goal of these trials was to apply pressure to a solidifying steel casting to improve soundness and mechanical properties.

2. Pressurized Casting Trial Procedures

The “platypus” casting selected for the pressurization trials is shown in Figure 2 as the gray object. The platypus casting utilized for material production qualification [5] and has been used recently to understand the dependency of mechanical properties based on manufacturing conditions [6]. The castings in this trial are produced in printed sand molds. The dimension of the “bill” width of the casting is 12.2” as shown in Figure 2(a) as a scale of the casting size. The rigging shown in Figure 2(a) was designed to produce steel with a range of mechanical properties representative of commercial castings. Castings produced with this rigging should have a range of soundness with sections having ASTM radiographic testing levels of 3 or better. For the pressurization trials it was decided to produce castings having more porosity than this; intentionally make an underfed casting. By doing this, the effect of pressure in reducing porosity should be more evident when the radiographs of the unpressurized and pressurized castings are compared. The casting solidified under atmospheric pressure is termed the “unpressurized” casting. To increase the porosity level in the casting for the trial, the bill feeder was removed from the casting. In addition, the gating was removed to reduce mold size for fitting into the vessel and to accommodate a bottom pour ladle with the casting filled by pouring into the side feeder. No hot topping was used.

To compare the effect of pressurization, the unpressurized and pressurized castings were radiographed. Eight radiographic views were used as shown Figure 3. This figure gives the x-ray orientations/directions for views 1 and 2 in Figure 3(a), view 2A (an orthogonal view to View 2) in Figure 3(b), and views 3 through 7 in Figure 3(c) inspecting the wall around the perimeter of the 3” thick ring feature of the castings. In the results section, the radiographs are given comparing un-pressurized and pressurized casting with each other and with simulations performed using a feeding porosity model that considers the effects of pressure [7].

In May 2024 the pressurized casting trials were poured at HS. Two platypus castings were produced from 8630-type quenched and tempered steel (Table 1), and one was pressurized. An identifying “SP” was stamped into the pressurized casting, and an “SA” marking was used for the casting solidified under atmospheric pressure. The casting was pressurized by placing it in a pressure vessel after pouring. The pouring times were 15 and 12.6 seconds for the pressurized and unpressurized castings, respectively. For the pressurized casting, pressurization began 51 seconds after the start of pouring, after the casting was placed into the vessel and the vessel was sealed. The maximum pressure of 10 atmospheres (150 psi) in the vessel was reached 125 seconds after the start of pouring. This pressure was applied for 25 minutes until the casting was solidified.

Table 1: Platypus chemistry

C	Mn	P	S	Si	Ni	Cr	Mo
0.27366	0.96959	0.02016	0.00931	0.44905	0.47989	0.49926	0.21742

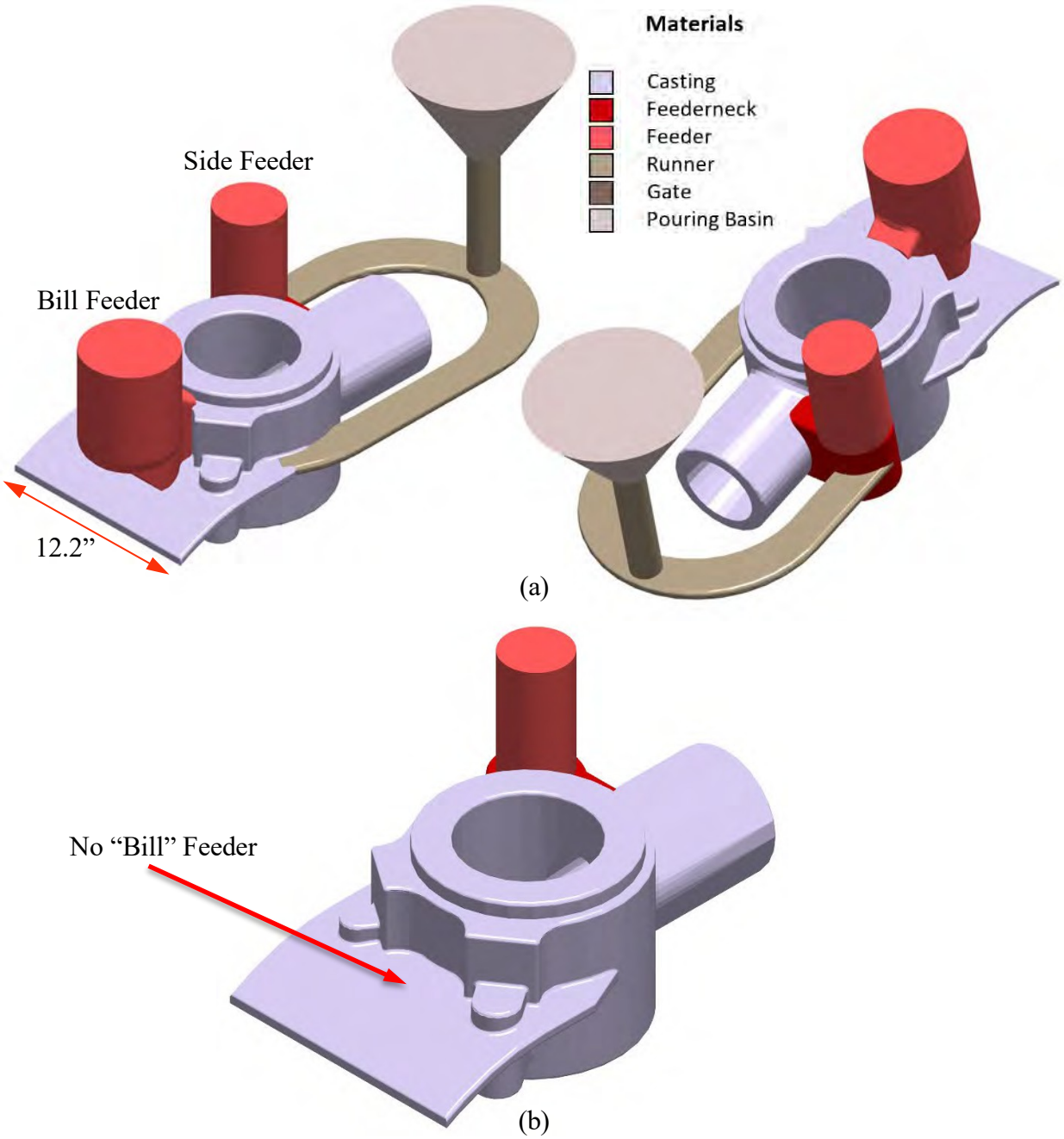

Figure 2 Solid models of the platypus casting rigging with gating system and two feeders (a). This rigging is designed to produce steel with mechanical properties representative of commercial castings [1]. Platypus casting rigging with only the side feeder as used in the pressurization trials (b).

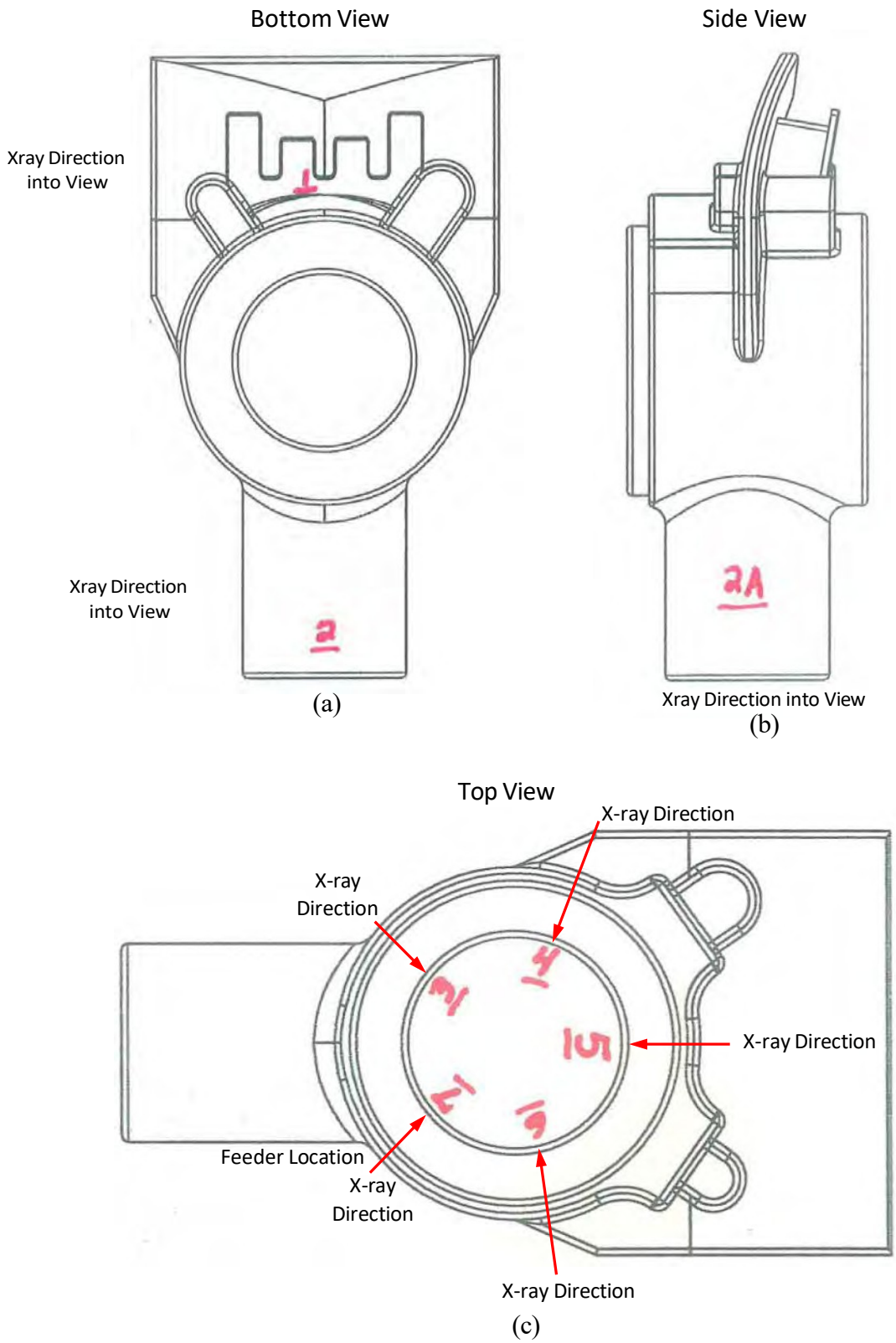

Figure 3 X-ray orientations/directions for views 1 and 2 (a), view 2A (b), and views 3 through 7 (c).

HS also cast the UAB wedge casting. A simplified pattern (Figure 4) was used; no chill at the bottom and no gating. Similar to the platypus, it was cast in an 8630-type alloy (Table 2) both unpressurized and pressurized. The pouring times were 5 seconds for both the pressurized and unpressurized castings, respectively. For the pressurized casting, pressurization began 40 seconds after the start of pouring, after the casting was placed into the vessel and the vessel was sealed. The maximum pressure of 10 atmospheres (150 psi) in the vessel was reached 135 seconds after the start of pouring. This pressure was applied for 22:43 minutes until the casting was solidified.

Figure 4: Vertically parted UAB wedge pattern

Table 2: Wedge chemistry

C	Mn	P	S	Si	Ni	Cr	Mo
0.2244	0.64663	0.01712	0.01039	0.46886	0.43557	0.50126	0.19318

Waukesha Foundry cast a plate casting in both CF3 and CF3M (Figure 5 and Table 3). The alloys were selected not based on mechanical properties but as they were common heats being produced to best enable doing the trial. Also, the plate pattern was owned by the foundry and rigged to produce sound test material (Figure 6). Therefore, this trial was intended to look primarily at reduced microporosity or smaller grains due to faster cooling rate. Pressure was applied for 15 minutes. Heat mechanical properties for CF3 was 79.8-40.1-46.0-63.3 and CF3M was 74.0-35.5-51.0-73.0.

Figure 5: Pressure trial of plate casting at Waukesha Foundry

Table 3: Plate chemistry

	C	Mn	P	S	Si	Ni	Cr	Mo
CF3	.026	.42	.014	.007	1.11	8.65	20.1	.12
CF3M	.020	.40	.029	.002	1.12	10.7	17.8	2.17

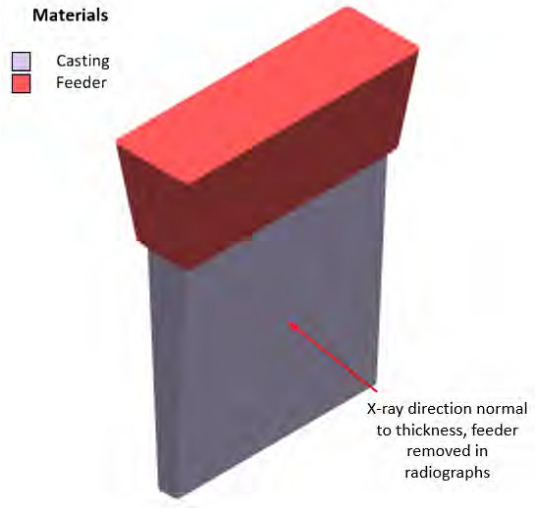

Figure 6: Waukesha Foundry plate casting and x-ray direction

3. Results

3.1 Results of Radiography and Castings Simulations

The first platypus simulation result shown is the hot spot criterion results in Figure 7. It is shown first to demonstrate the fundamental solidification conditions in the part that pressurization cannot change or overcome. The hot spot criterion results show two hot spot regions (high values of the criterion): one at the side feeder contact inside the casting, and the other in the ring along the bill, where the bill feeder contact would be. Considering this result, it is difficult to see that the hot spot at the bill could be fed, even with pressure, as it will be isolated from the pressurized feeder. Also, with the bill feeder removed, the only feeder in the rigging is the side feeder. It is inadequately sized to feed all the solidification shrinkage in the casting. So, the shrinkage piping in the side feeder is expected to extend into the casting regardless of pressure.

Radiographs and porosity predictions in x-ray view from views 1, 5 and 2 in Figure 2 are shown in Figure 8, Figure 9 and Figure 10, respectively. Results are shown for the unpressurized and pressurized castings.

The key observation from the unpressurized versus pressurized radiographs in Figure 8(a) is that circular-shaped gas porosity is seen in the unpressurized casting. This porosity forms early during solidification in the mostly liquid steel as spheroidal shaped porosity. The effect of pressure is to either prevent the formation of, or to heal, this porosity given its absence in the pressurized castings. As will be observed in the results to follow, this gas porosity suppression is found to be the main effect on the porosity seen in the radiographs when comparing pressurized versus unpressurized castings. In Figure 8(b), the porosity predicted in the ring is not visible in the radiograph due to the thickness of the ring section. This porosity prediction is very similar regardless of pressurization. The main difference is that two regions of porosity are seen for the unpressurized casting. Note there is also dispersed microporosity predicted in Figure 8(b) for the unpressurized casting. Finally, be aware that the porosity model used here [8] predicts porosity forming from calculation of shrinkage and pressure driven flows. It does not predict gas porosity.

The radiographs for view 5 in Figure 9(a) show large areas of shrinkage porosity for both castings. Only the unpressurized casting also has areas of gas porosity in the radiographs above the shrinkage porosity. The porosity predictions in Figure 9(b) shows the unpressurized casting with two separate regions of macroporosity and some dispersed microporosity. The pressurized casting has one central region of macro porosity. The differences in the macroporosity predictions between the two castings are not thought to be meaningful. What is meaningful is that porosity forms in the hot spot location as discussed above that the pressure cannot prevent from forming.

In Figure 10(a) the radiograph for view 2 for the unpressurized casting shows many gas porosity indications while the pressurized casting shows one location that might be gas porosity. That location might also be a surface/inclusion defect. Either way, again the pressurized casting id nearly completely free of any indications. The x-ray view of porosity predictions in Figure 10(b) show nearly identical macroporosity associated with the side feeder shrinkage piping. The only difference between the two castings seen in Figure 10(b) is the dispersed microporosity predicted in the unpressurized casting.

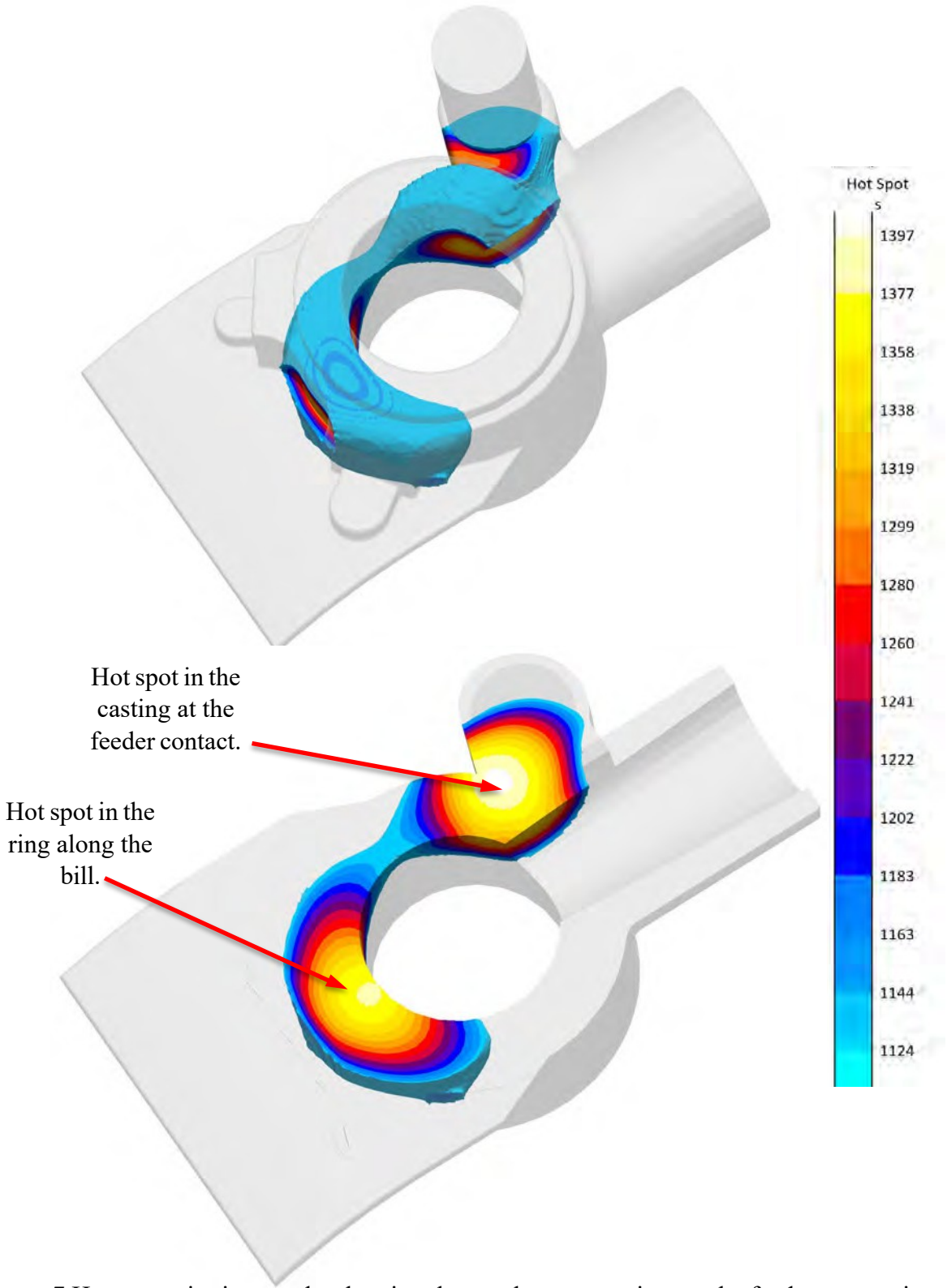

Figure 7 Hot spot criterion results showing the two hot spot regions at the feeder contact in the casting, and in the ring along the bill.

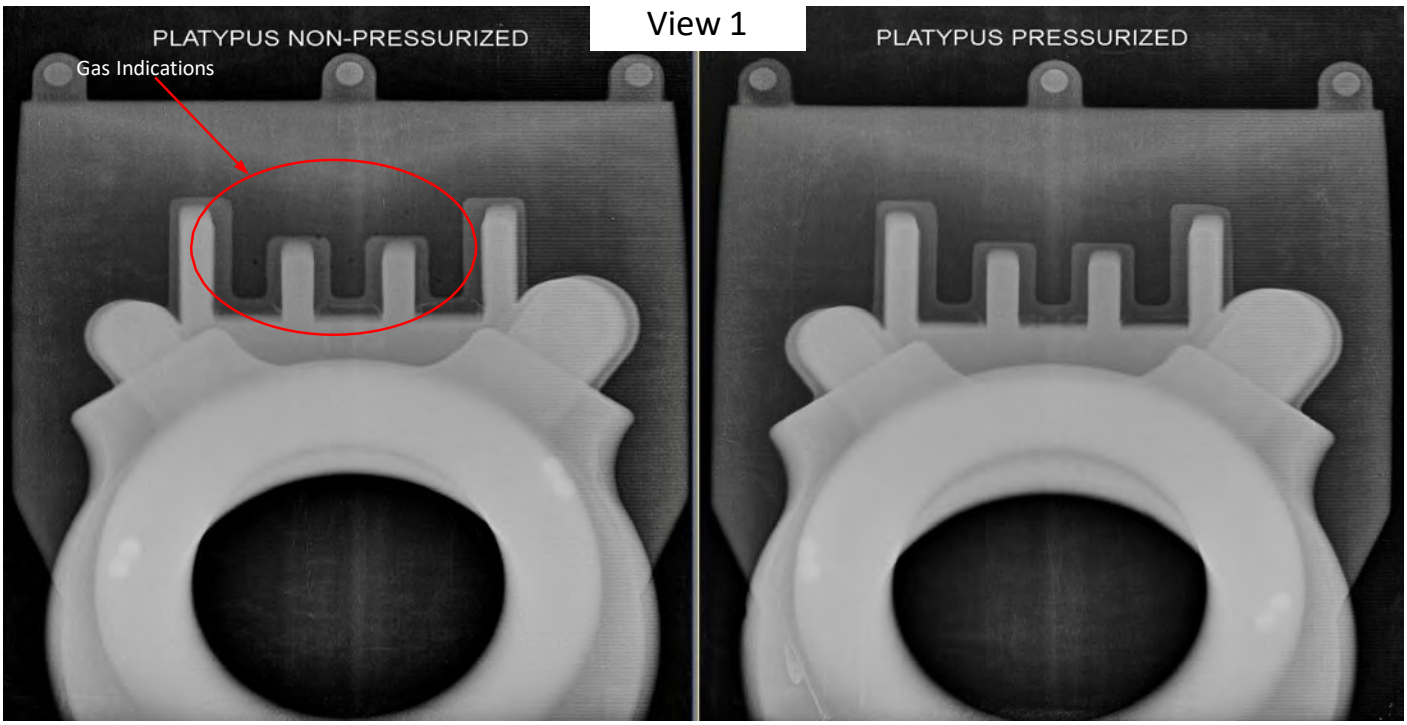

(a)

Un-Pressurized at 1 atm (14.7 psi)

Pressurized to 10 atm (150 psi)

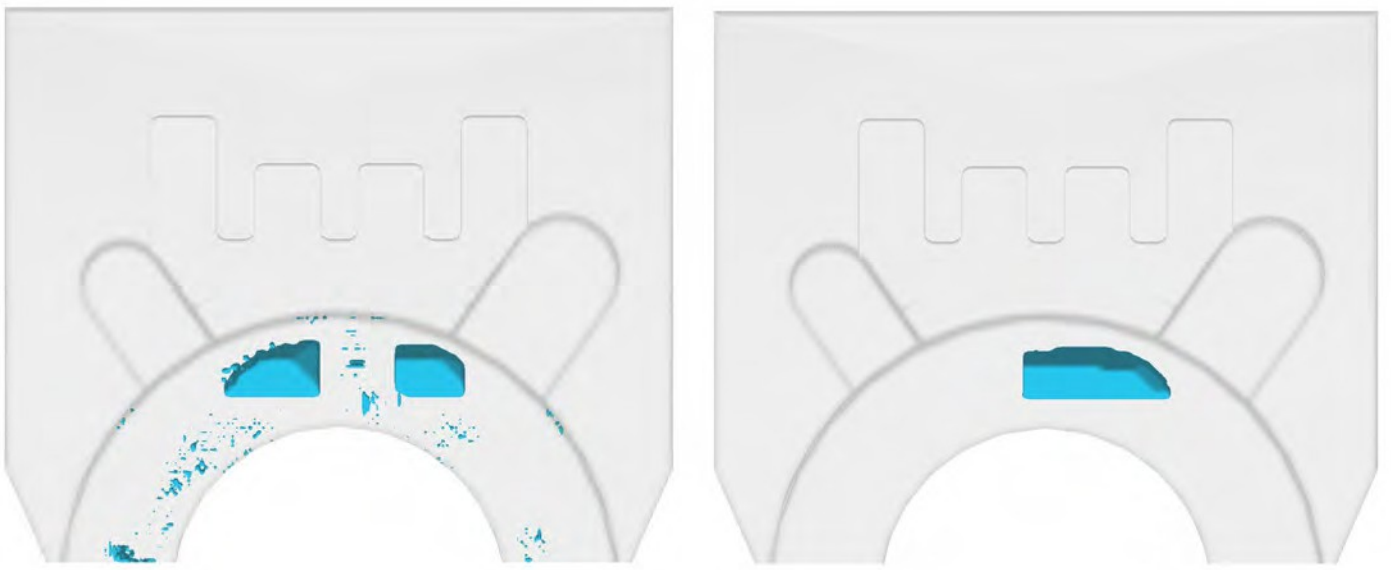

(b)

Figure 8 Radiographs from View 1 of un-pressurized and pressurized castings (a) and x-ray views of predicted porosity without and with pressure (b).

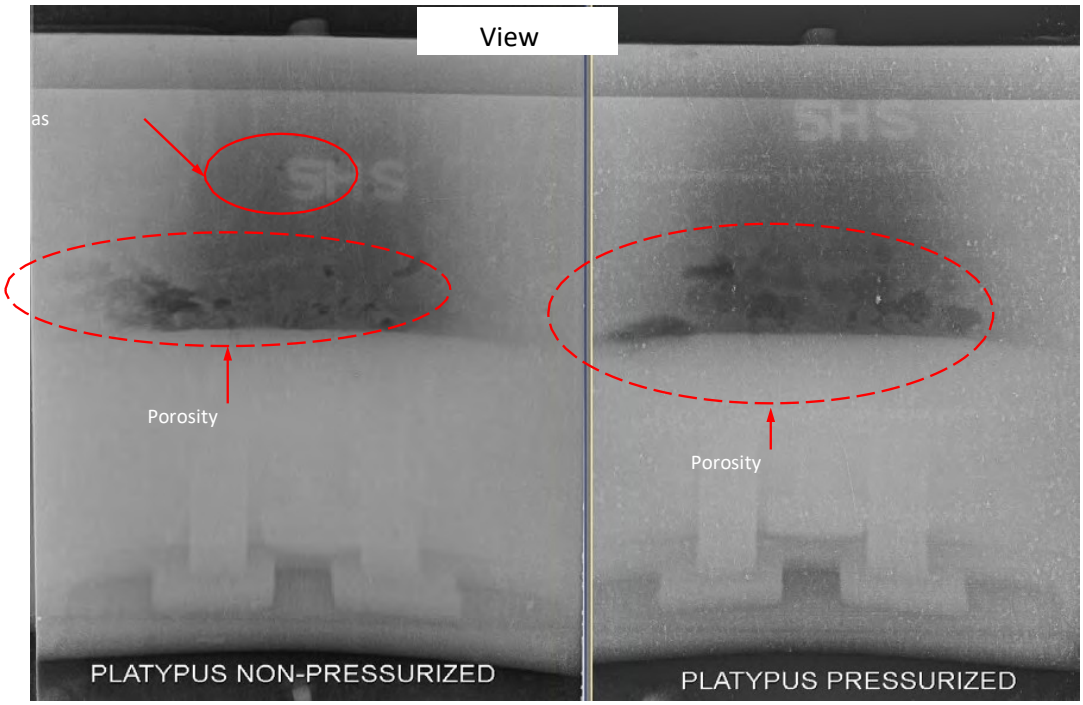

(a)

Un-Pressurized at 1 atm (14.7 psi)

Pressurized to 10 atm (150 psi)

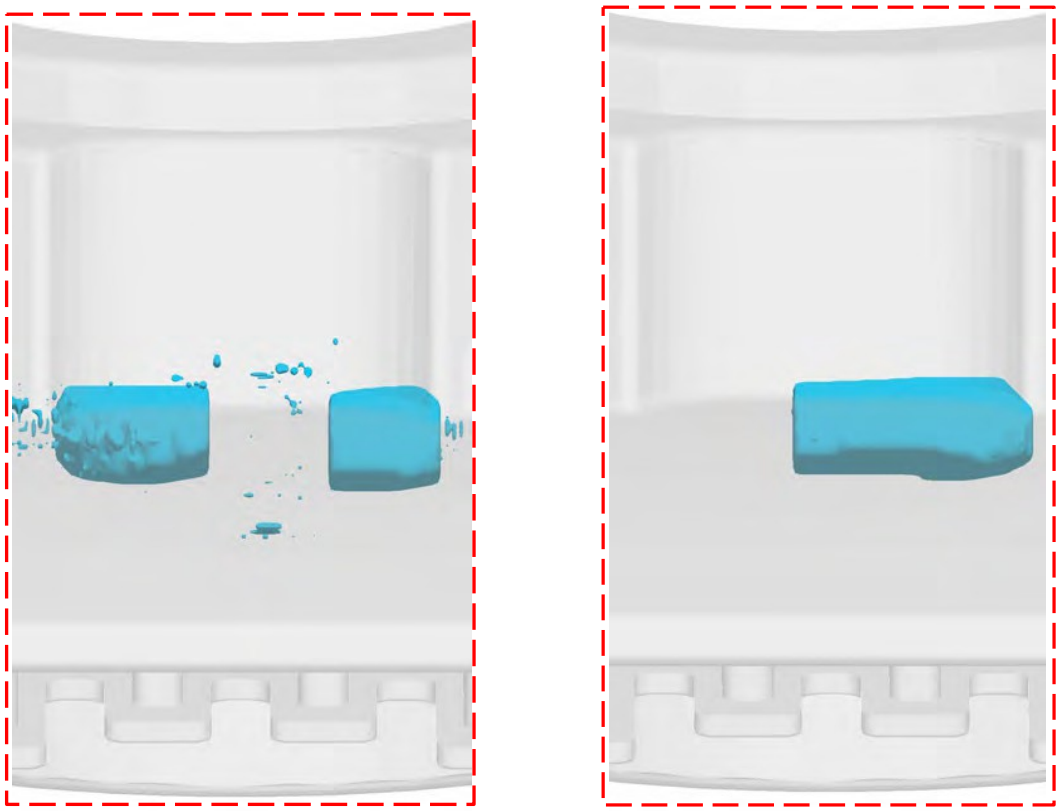

(b)

Figure 9 Radiographs from View 5 of un-pressurized and pressurized castings (a) and x-ray views of predicted porosity without and with pressure (b).

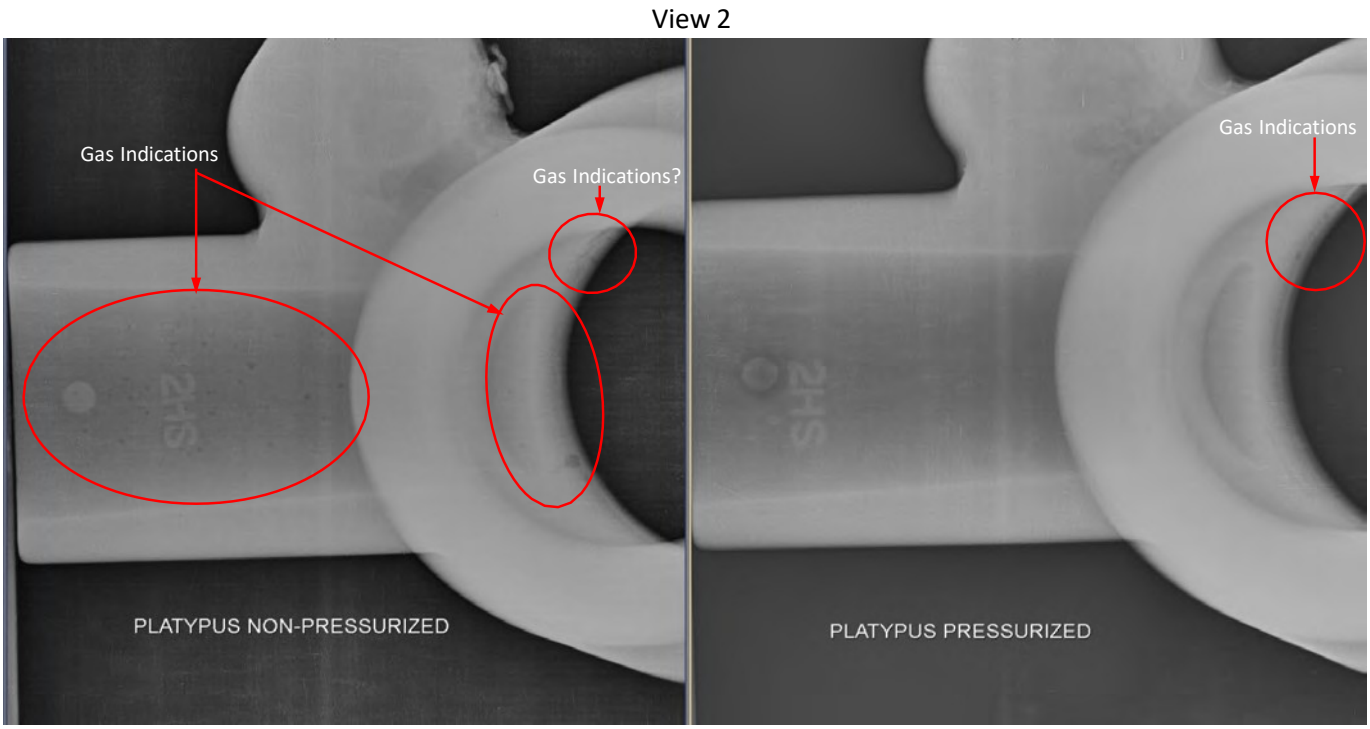

Figure 10 Radiographs from View 2 of un-pressurized and pressurized castings (a) and x-ray views of predicted porosity without and with pressure (b).

In Figure 11, Figure 12 and Figure 13 the remaining radiographs for the views shown in Figure 3 are provided for the unpressurized and pressurized castings. The figures give the unpressurized/pressurized results side-by-side for each view. Again, numerous gas porosity indications are observed for the unpressurized casting and only a few indications are seen in the pressurized casting. In the radiographs, many indications appear to have tracks to the casting cope surface. These indications are circled in Figure 11(b), Figure 12(a) and Figure 12(b) and Figure 13 at the top end of the radiographs for views 3, 4, 6 and 7, respectively. Holes from these indications were observed on the casting cope surfaces. Some gas indications associated with inclusions have an appearance like this. They leave gas trails tracing their paths in the casting. The radiographs for view 4 (Figure 12(a)) and view 6 (Figure 12(b)) both show larger porosity indications for the unpressurized castings which are most likely gas, but might also be shrinkage porosity. For the pressurized casting no indications are detected in Figure 12. The benefits of pressure are clear in this figure whether it is suppressing or healing gas or shrinkage porosity. Differences are seen in the shrinkage of the feeders in Figure 13 between the unpressurized and pressurized castings. Sectioning of the castings vertically at the feeder might have reveal the effects of pressure on the feeder piping. However, this has yet to be performed as of the writing of this paper.

Simulation results for porosity are shown in Figure 14 and Figure 15 for the unpressurized and pressurized castings. In Figure 14 x-ray views of the in one orientation for the unpressurized casting in (a), and the pressurized casting in (b). Side views of the same results are given in Figure 14(c) and Figure 14(d). Figure 14 is provided to give a more complete visualization of the porosity distribution predicted in the two castings. A horizontal slice through the unpressurized and pressurized castings showing the porosity results using a sensitive microporosity scale is given in Figure 15. This figure provides a comparison of the microporosity predicted on the section slice. The applied pressure is predicted to greatly reduce the microporosity in the casting on the section slice with one spot on the section surface predicted.

Simulation results exploring the effect of pressure on feeding flows are discussed in the final part of this section. First the predicted solid fraction with superimposed feeding velocity vectors on a horizontal plane section for the unpressurized casting is shown in Figure 16 at three points during solidification. In the figure the solid fraction results are shown at 82%, 92% and 96% of the total solidification for the entire casting system (feeder and casting). Location of the feeding flow cut off from the feeder to the hot spot in the ring/bill intersection is shown in Figure 16. The three points during solidification are selected because at 82% in Figure 16(a) the solid fraction at the cut off point has a minimum solid fraction around 60% solid. At this point the feed path is still open between the feeder and the hot spot, and the velocity vectors indicated the flow is strong in the direction of the hot spot from the feeder. In Figure 16(b) at 92% solidified, the fraction solid is around 80%. The velocity vectors still indicate that the flow is continuous from the feeder to the hot spot. Then at 96% solid in Figure 16(c), the flow is cut off and the flow directions are from the hot spot and the feeder to the cut off location from both sides. So, for the unpressurized casting (simulated with a pressure of 1 atmosphere) the feeding flow is cut off between 92% and 94% total solidification. It was observed that at 94% solid the porosity at the hot spot forms rapidly for the unpressurized casting.

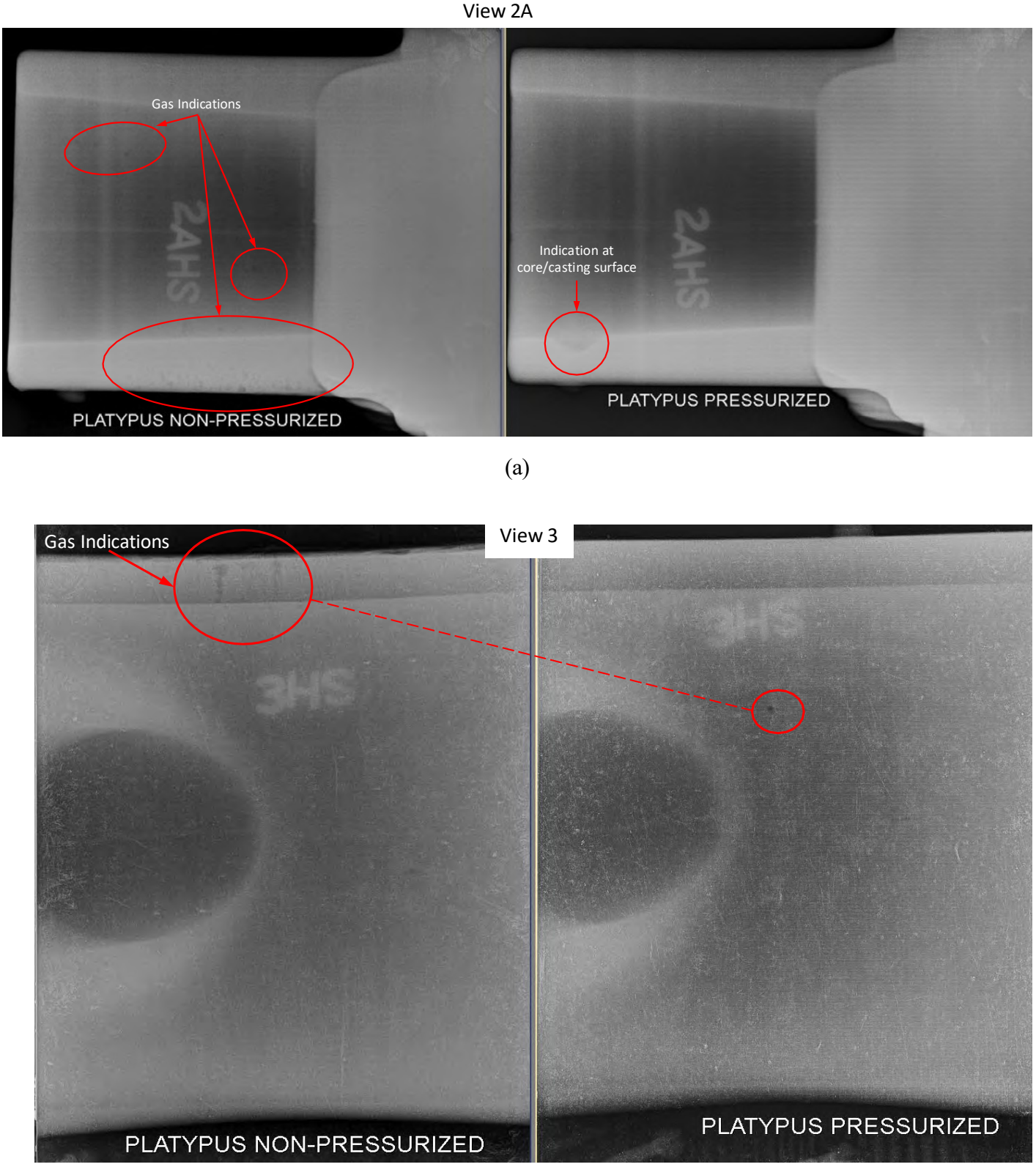

Figure 11 Radiographs from View 2A of un-pressurized and pressurized castings (a) and radiographs from View 3 of un-pressurized and pressurized castings (b).

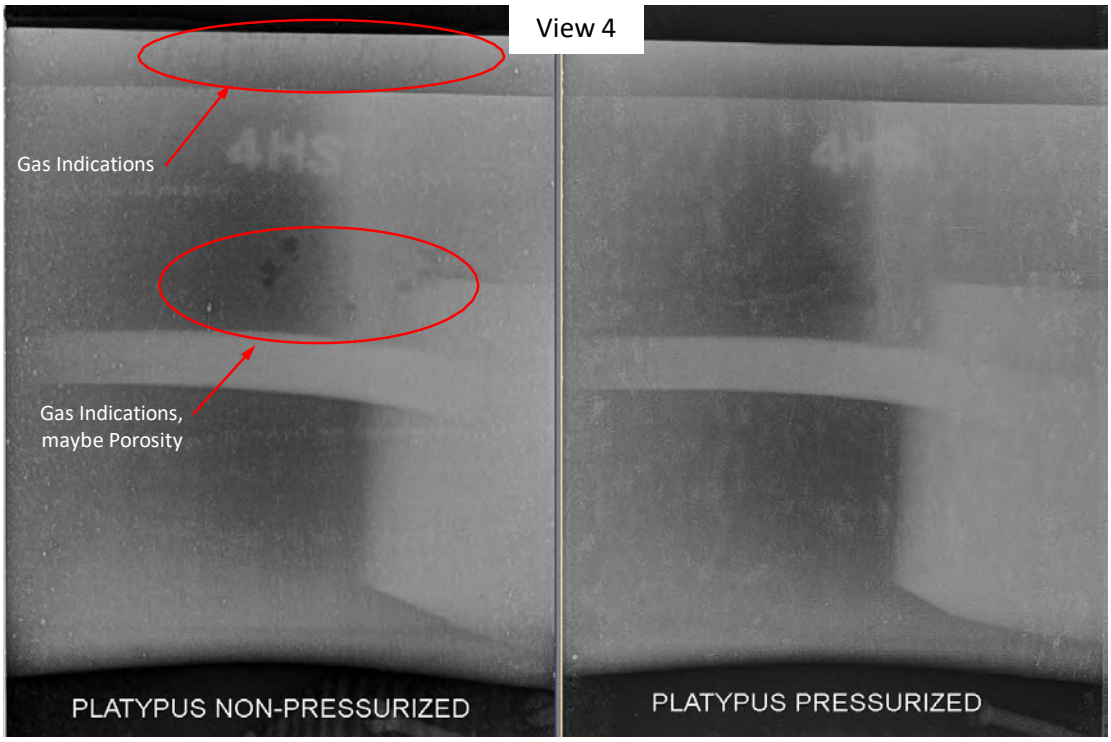

(a)

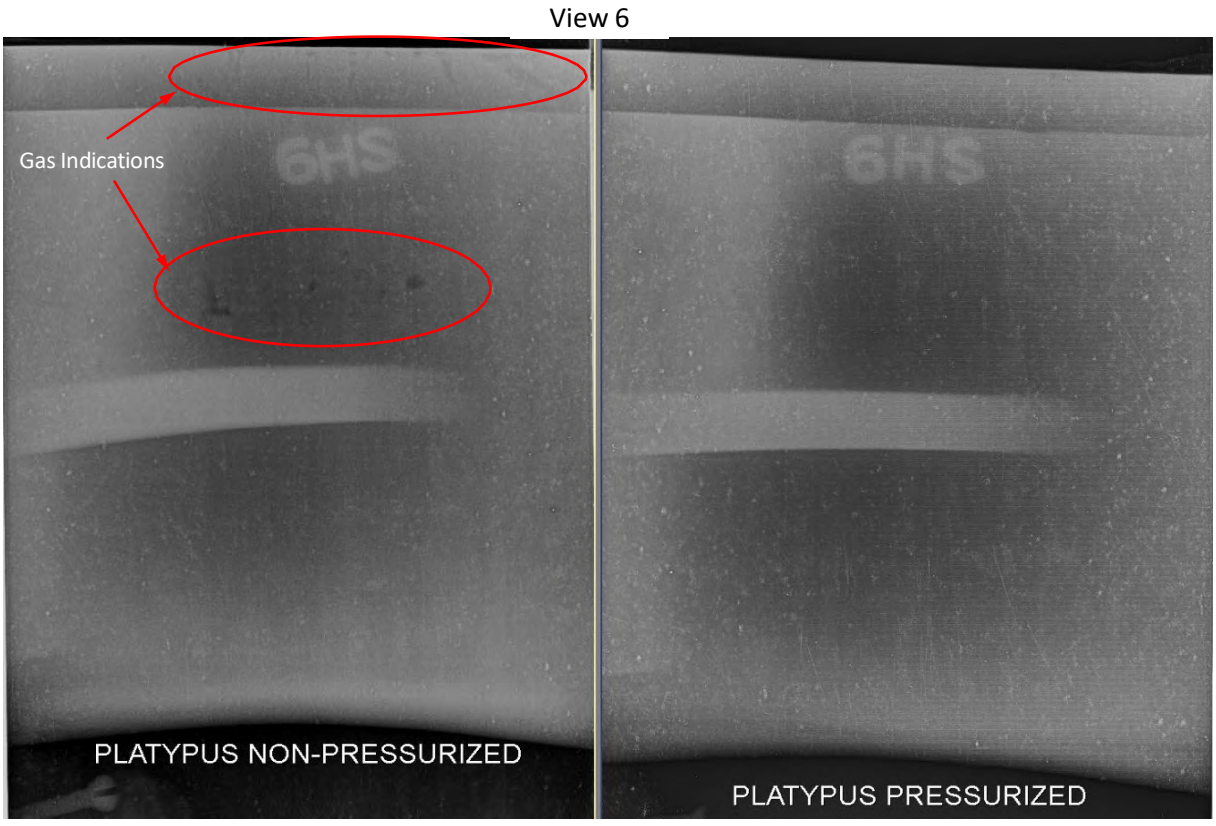

(b)

Figure 12 Radiographs from View 4 of un-pressurized and pressurized castings (a) and radiographs from View 6 of un-pressurized and pressurized castings (b).

View 7

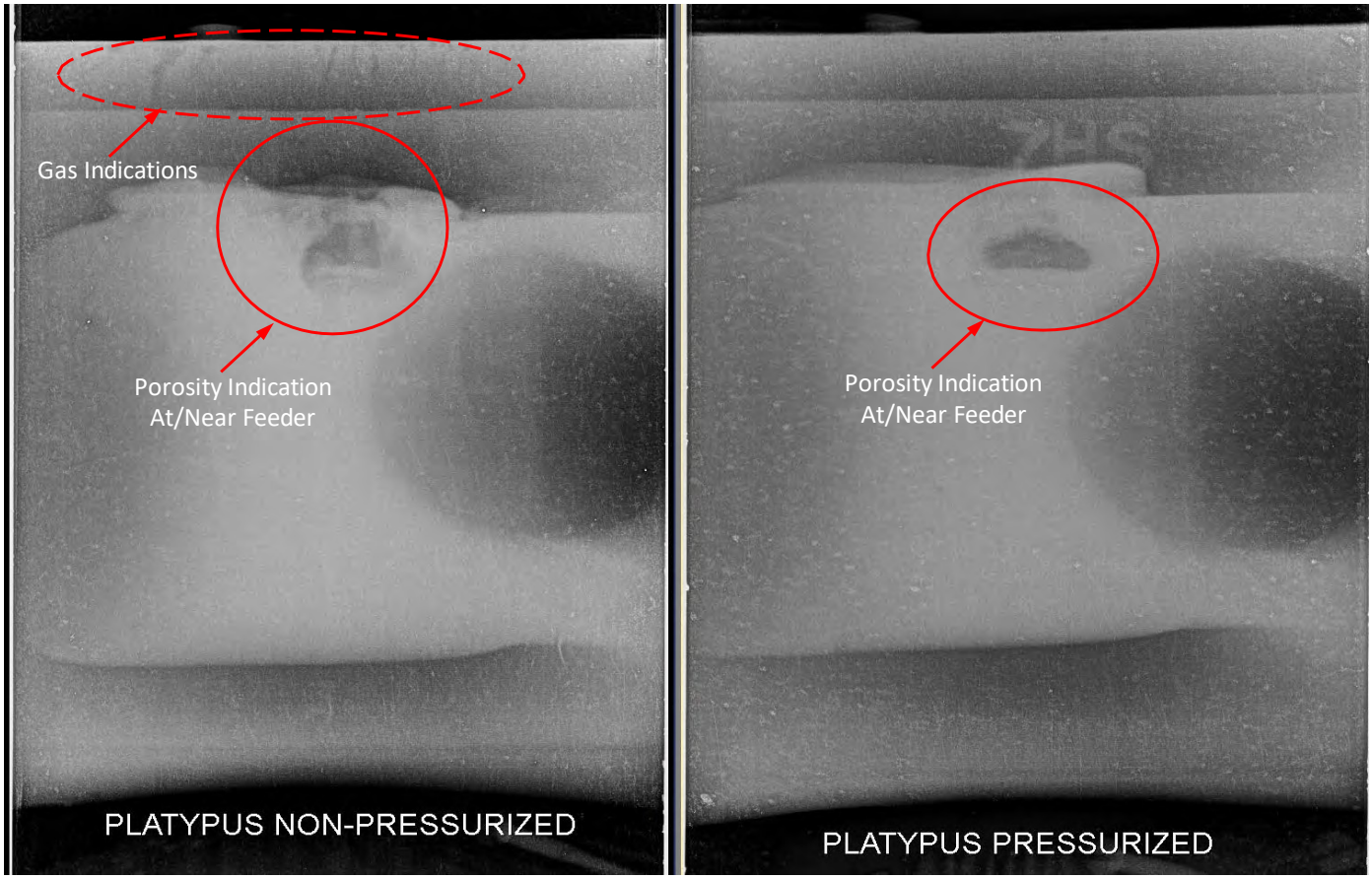

Figure 13 Radiographs from View 7 of un-pressurized and pressurized castings.

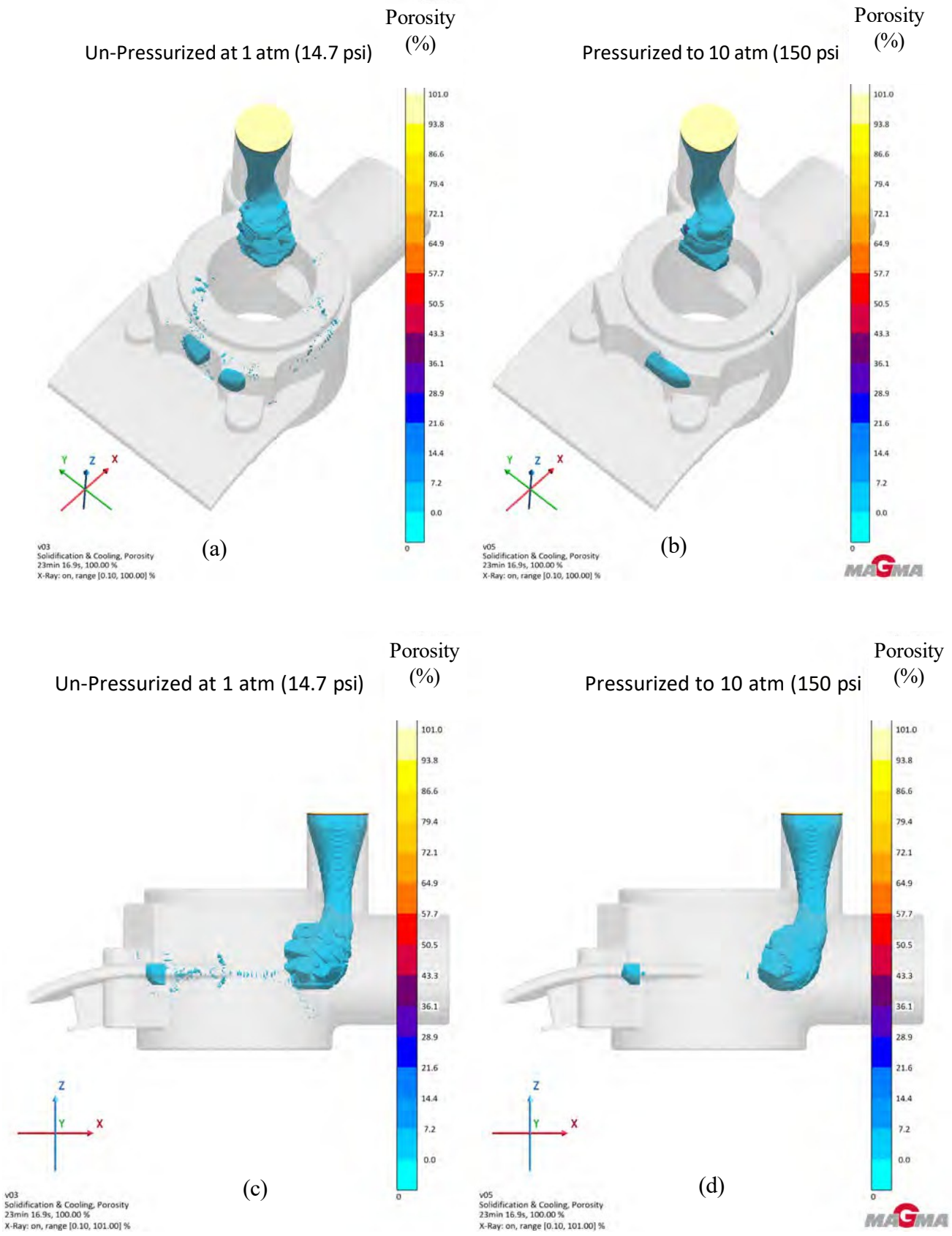

Figure 14 X-ray views of final porosity predictions in the unpressurized casting (a), the casting pressurized to 10 atm (150 psi), and side views of the same (c) and (d).

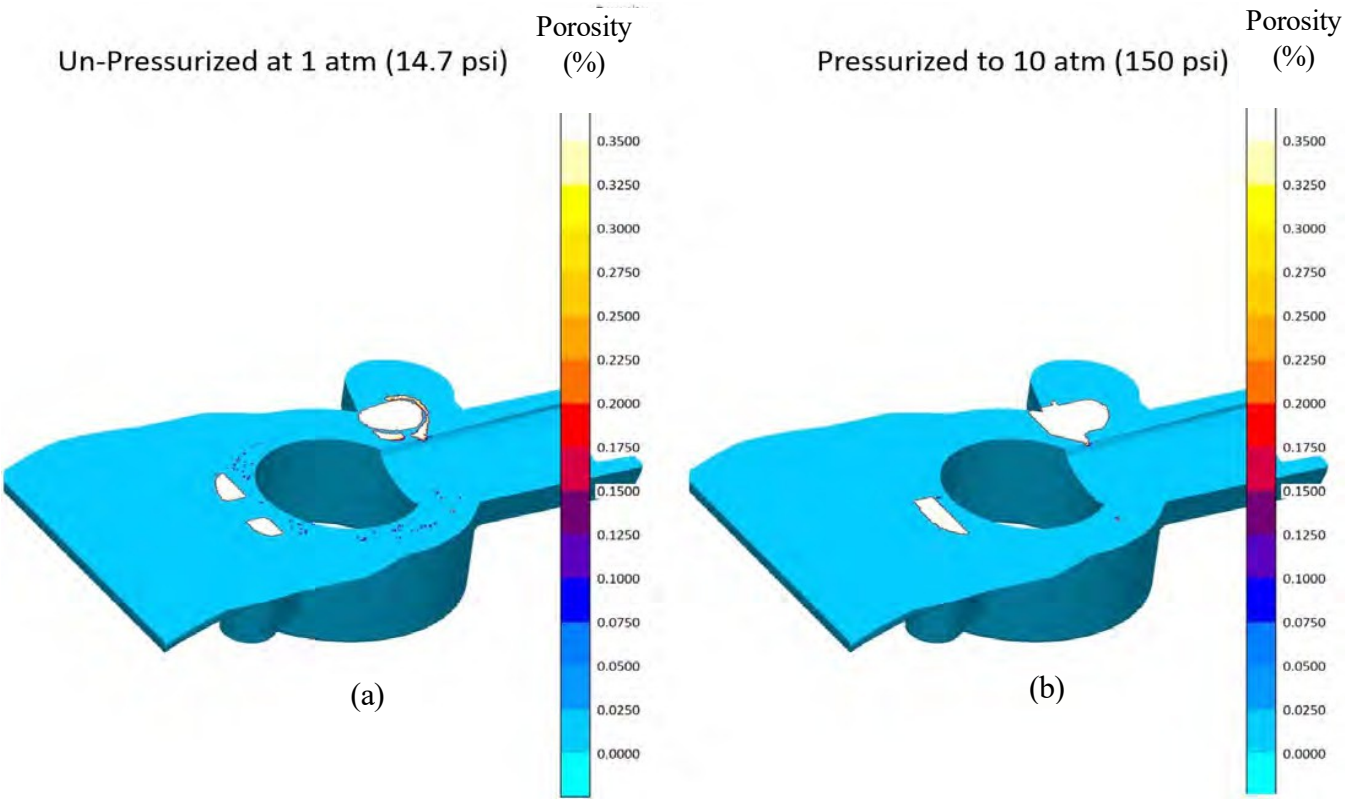

Figure 15 Horizontal section views through the final porosity predictions in the unpressurized casting (a) and the casting pressurized to 10 atm (150 psi).

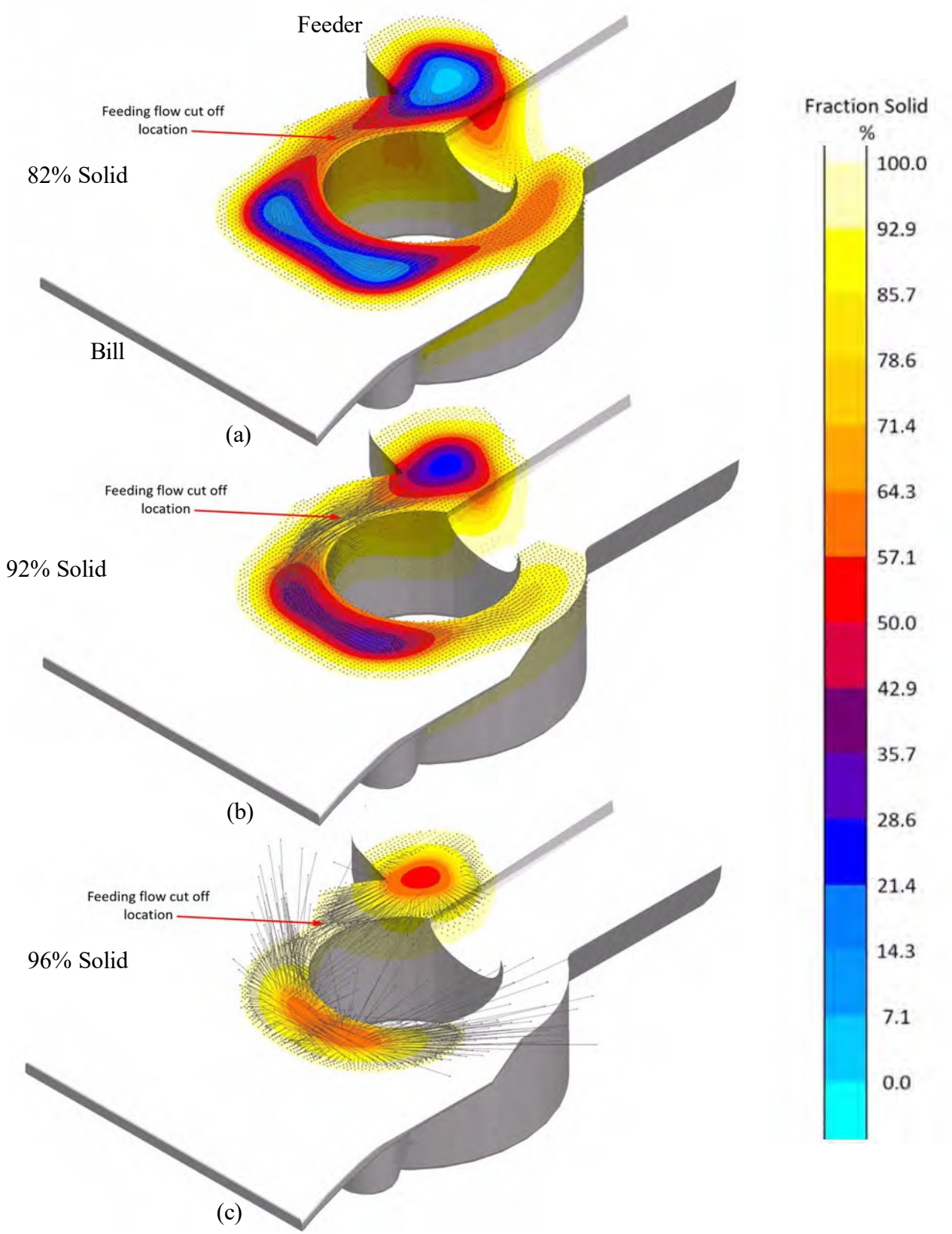

Figure 16 Predicted solid fraction with superimposed feeding velocity vectors on a horizontal plane section for the unpressurized casting. Results are shown at 82%, 92% and 96% of the total solidification. Location of the feeding flow cut off is shown.

The simulation and feeding flow results for the pressurized and unpressurized casting are compared in Figure 17 and Figure 18. The results in the figures are given at the time that the feeding flow is cut off to the hot spot for the unpressurized casting (94% total solidified), and at a time close to the flow cut off for the pressurized casting at 96% solidified. In Figure 17 the velocity magnitude results are given. The velocity magnitude is the square root of the sum of the three velocity components squared. In Figure 17 the maximum velocity on the legend scale is $1x10^{-6}$ m/s (or $1x10^{-3}$ mm/s). So the feeding flow is a slow creeping flow. At 94% solidified in Figure 17(a) and (b), the unpressurized casting feeding velocities are much lower than the pressurized casting, and they decrease even more (to 0 m/s) at the hot spot. This is more data supporting the feeding cut off for the unpressurized casting at 94% solidified (or 939 seconds from the start of pouring). In Figure 17(b) the pressurized casting feeding velocities are much higher and the hot spot is still being fed. At 96% solidified (or 1016 seconds from the start of pouring), the unpressurized casting in Figure 17(c) has very low feeding velocities isolated to the hot spot area. While the pressurized casting in Figure 17(d) still shows velocities feeding the hot spot from the feeder, but they are much lower than at 94% solidified and the feeding flow is being cut off. For the pressurized casting, it can be conservatively estimated that the feeding flow is cut off at 96%. Given the time difference between 94% and 96% solidified, the application of pressure is predicted to give an additional 77 seconds of flow from the feeder (calculated from 1016 minus 939 seconds).

Calculated pressure fields are given in Figure 18. These results correspond to the same pressurization conditions and points in the solidification process as shown in Figure 17. In Figure 18(a) and (b) the predicted pressure distributions are shown on a horizontal plane section at 94% of the total solidification for the un-pressurized and pressurized castings, respectively. Then in Figure 18(c) and (d) the pressure distributions are shown at 96% solidified for the unpressurized and pressurized castings, respectively. For the unpressurized casting in Figure 18(a) and (c), there is virtually no difference in the pressure fields as solidification progressed. For this casting the pressure of the feeder is atmospheric (1034×10^2 Pa) as seen in these results. Again, note that the feeding is cut off as is demonstrated by the pressure at the hot spot being below 0 (or vacuum pressure). For the pressurized casting in Figure 18(b), there is a relatively small pressure drop through the solidifying steel “mush.” The pressure is communicated to the hot spot zone. Liquid is pushed to the hot spot zone. Then at 96% solidified, in Figure 18(d), the pressure drop and gradient across the mush to the hot spot zone is extremely large, from 10 atmospheres to vacuum. The feeding flow from the feeder to the hot spot is cut off. Clearly the pressurization of the casting has an effect on feeding by extending the time the feeder is active in the process. The benefits of pressure are only marginal in feeding the hot spot in this case. It is recommended that the new modeling capabilities presented here [7,8] be used to design future pressurization trials and experiments to showcase its advantages.

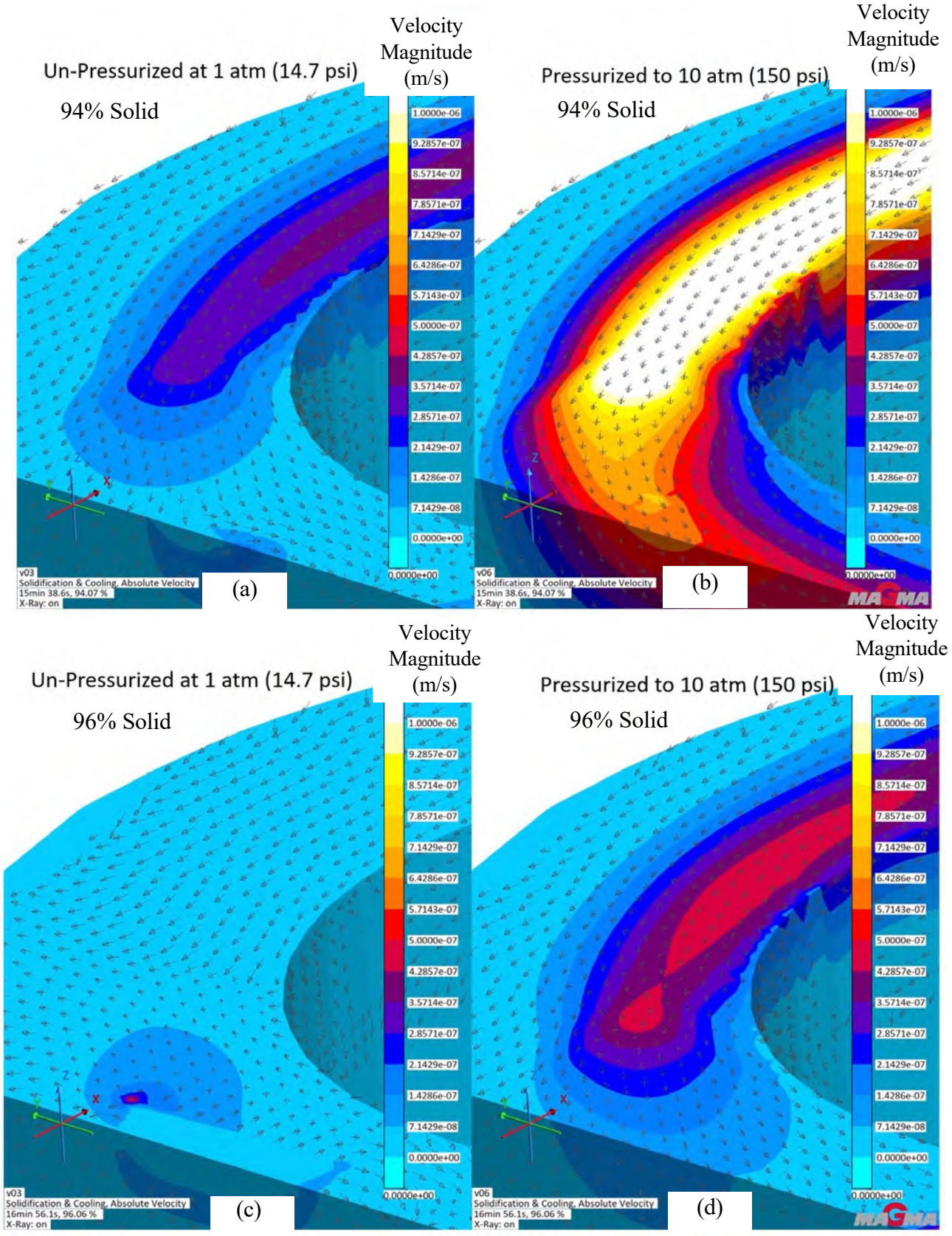

Figure 17 Predicted velocity magnitude with vectors on a horizontal plane section at 94% of the total solidification for the un-pressurized (a) and pressurized (b) casting. Same results shown at 96% solidified for the unpressurized (c) and pressurized (d) castings.

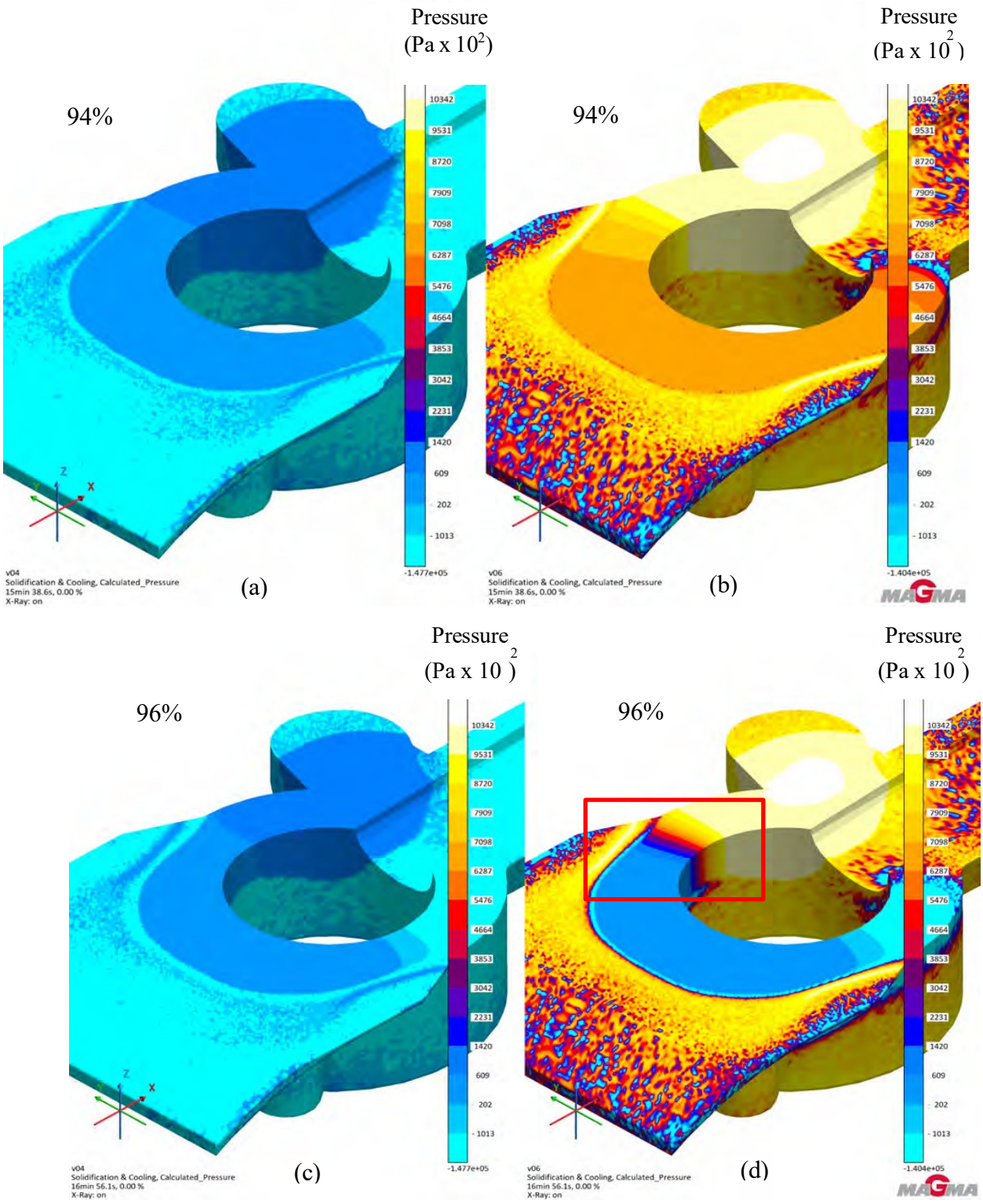

Figure 18 Predicted pressure distribution on a horizontal plane section at 94% of the total solidification for the un-pressurized (a) and pressurized (b) casting. Pressure distribution shown at 96% solidified for the unpressurized (c) and pressurized (d) castings.

The wedge x-rays show little difference between pressurized and unpressurized (Figure 19). In the radiographs, the feeder is at the top and was included in the shot; shrink is seen in the feeder.

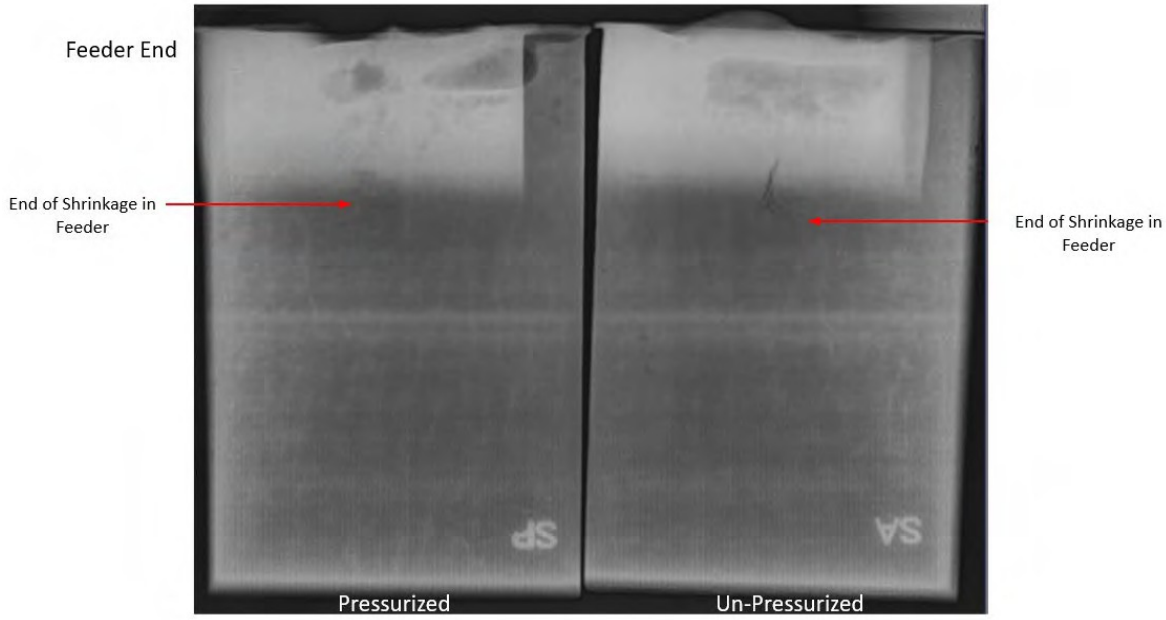

Figure 19: HS wedge casting x-rays

The plate x-rays (Figures 20 and 21) only show a difference in the unpressurized CF3 casting. The gas indication is at the center of the film and was noted as appearing to be open to the surface. All other indications were surface indications. The simulation shows no difference in porosity predicted between pressurized and unpressurized; both are sound. The only difference when pressure is applied is the predicted for the feeder shrink pipe.

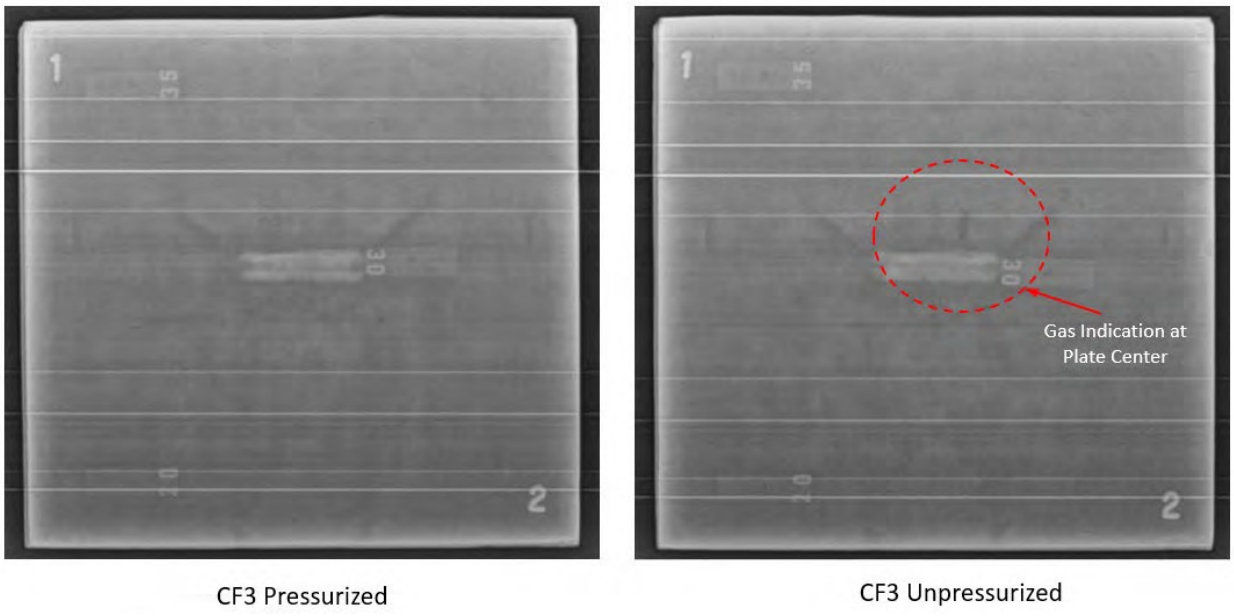

Figure 20: Waukesha Foundry CF3 plate casting x-rays

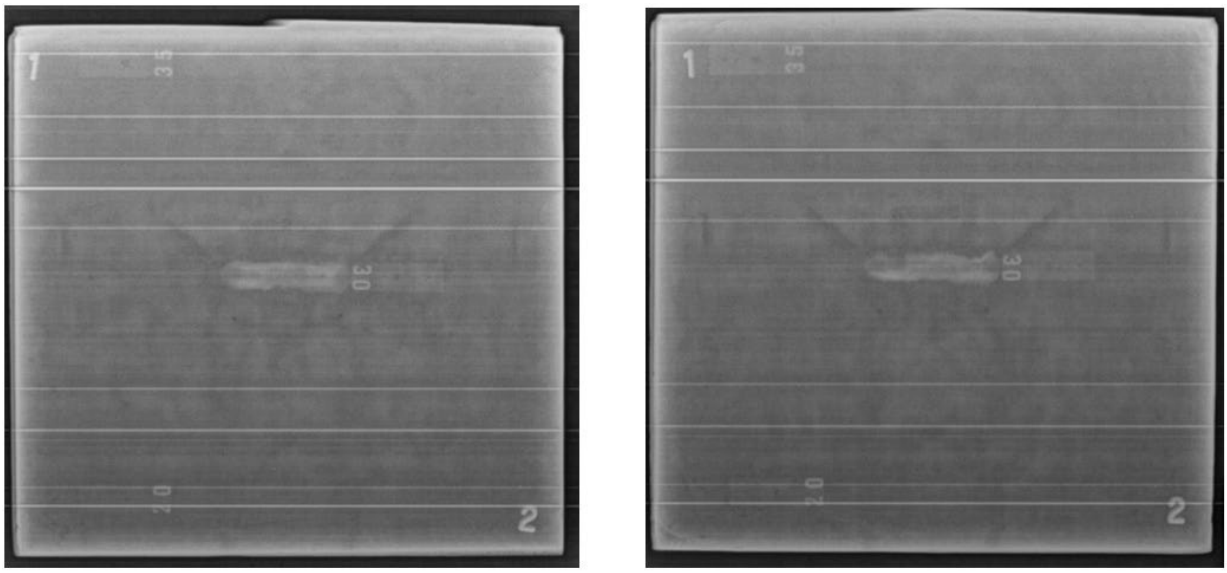

Figure 21: Waukesha Foundry CF3M plate casting x-rays

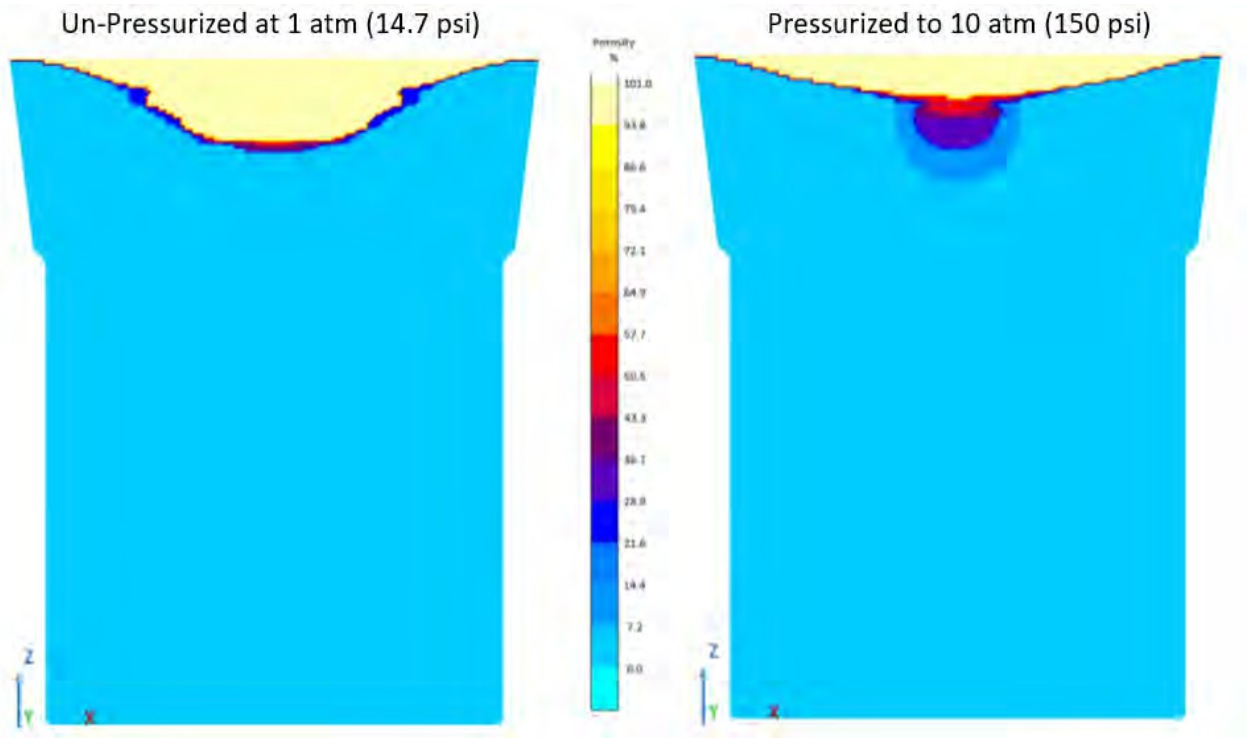

Figure 22: Plate porosity simulation for both pressurized and unpressurized

3.2 Comparison of Dimensions between Pressurized and Unpressurized Castings

Several dimensions were compared between the two trial castings to investigate what effect if any applying pressure had on the dimensions. The dimensions were measured by UAB, before the castings were sectioned to obtain tensile testing specimens. Four locations were selected for the measurements as shown in Figure 23. Three locations (locations 1 to 3) around the ring feature of the casting were selected for ring thickness measurements. The fourth location was a region of the bill selected or thickness measurements. In Figure 23 the measurement locations for platypus castings are indicated between the lines on the casting surface at locations numbered 1 to 4. These thickness dimensions were measured five times each at location.

Before looking into the analysis of the dimensions, note in Figure 23 the difference in appearance of the two castings. The surface of the unpressurized casting on the right is pock-marked with dimples on the ring and on the bill surfaces. On the ring these dimples are without doubt related to the gas defects observed in the radiographs discussed in the previous section. Conversely, the pressurized casting on the left in Figure 23 has no surface dimpling and is remarkably smooth by comparison to the casting on the right. Pressurization improved the appearance of the casting surface.

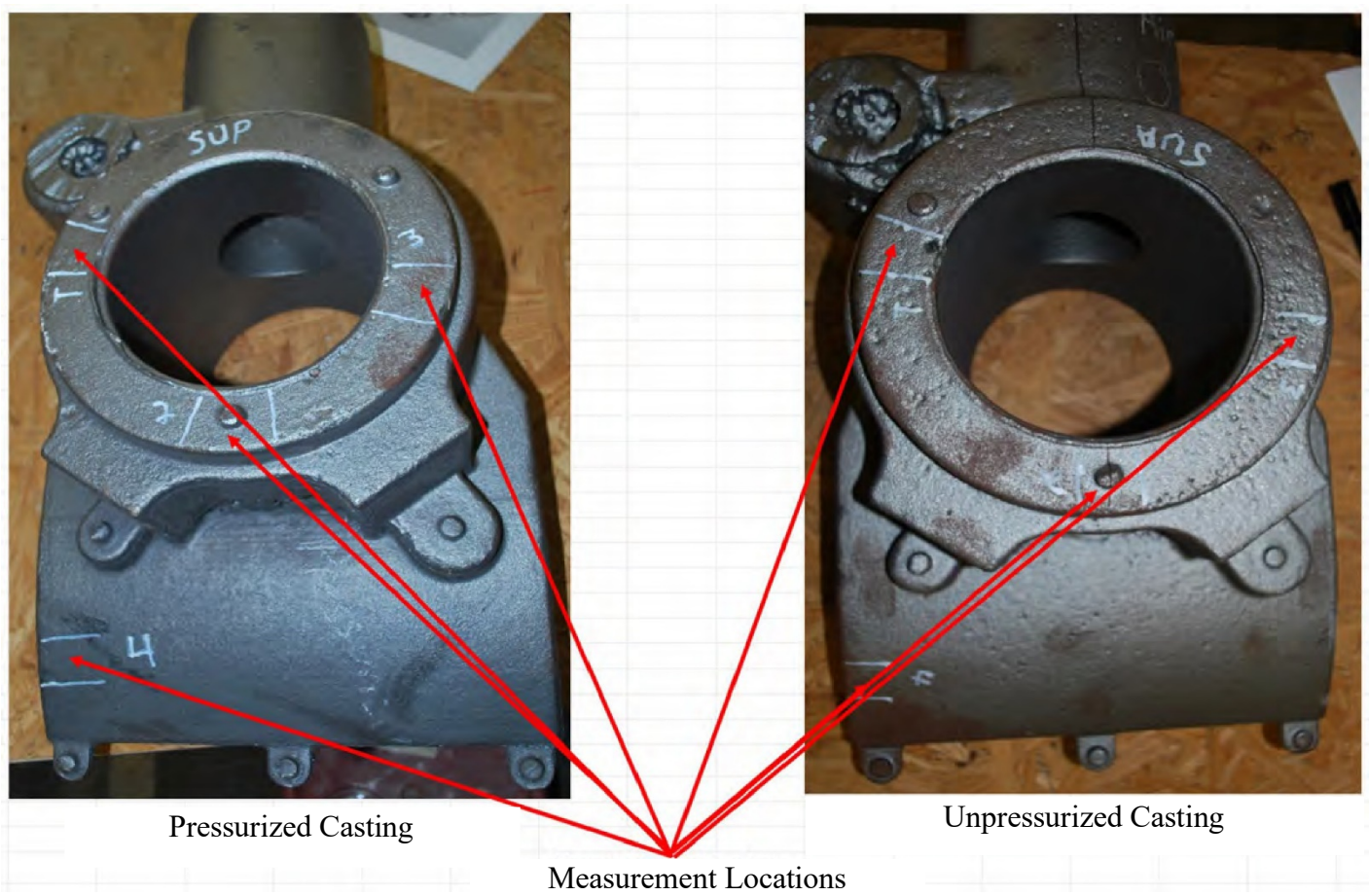

Figure 23 Measurement locations 1 to 4 for platypus castings indicated between the lines on the casting surface. Thickness of the ring is measured five times each at locations 1 to 3, and bill thickness measured 5 time at location 4.

In Table 3 the measured section thickness dimensions for the platypus castings are given arranged by location number, and whether the casting was pressurized (casting ID "SUP") or unpressurized (Casting ID "SUA"). The dimensions are given in millimeters. Five thickness measurements are given in the rows under each location. The average and standard deviation for each location and castings are given below the five measurements. The bottommost row in Table 4 is the difference in average dimensions, (pressurized dimension – unpressurized dimension). The specimen locations for the SUP and SUA castings are arranged side-by-side in the table for comparison. For example, looking at the red outlined boxes, for the case of location 1 the average pressurized/SUP casting dimension is 49.2 mm, and the average unpressurized/SUA casting dimension is 47.9 mm. Their difference is 1.3 mm. The pressurized dimension is much larger than the unpressurized dimension at location 1, and the opposite is observed at location 3. For the bill thickness at location 4, there is no real difference in the dimensions.

Table 4 Measured section thickness dimensions in millimeters for the platypus castings arranged by location number and whether the casting was pressurized (casting ID "SUP") or unpressurized (Casting ID "SUA"). Five thickness measurements are given in rows for each location. Average and standard deviation are below the fifth measurement. The bottommost row is the difference in average dimensions (pressurized – unpressurized).

	Casting ID and Location Number							
Measurement Number	SUP-1	SUA-1	SUP-2	SUA-2	SUP-3	SUA-3	SUP-4	SUA-4
1	49.0	47.9	48.9	48.9	48.2	49.5	16.2	16.2
2	49.1	47.8	49.0	48.8	48.1	49.4	16.1	16.0
3	49.0	47.9	49.1	48.7	48.3	49.4	16.0	16.1
4	49.2	47.9	49.2	48.7	48.2	49.5	15.8	16.1
5	49.5	48.0	49.5	48.7	48.3	49.4	15.8	16.1
Average	49.2	47.9	49.1	48.7	48.2	49.4	16.0	16.1
Std Deviation	0.2	0.1	0.2	0.1	0.1	0.0	0.1	0.1
Pressure - No Pressure	1.3		0.4		-1.2		-0.1	

The average dimensions in Table 4 at the four locations, for the two castings, are plotted in Figure 24 where the error bars are +/- one standard deviation from the table. Here in Figure 24(a) the pressurized dimensions at locations 1 and 2 are larger than the unpressurized dimensions. Also, the differences at locations 1 and 2 exceed the standard deviation. Again, at location 3 the pressurized dimension is smaller, and the difference between the castings exceed the standard deviation. Since the differences in the averages exceed the standard deviation by two to over ten times for these locations, the differences in the pressurized and unpressurized castings are significant. Finally, in Figure 24(b), no difference seen in the bill thickness at location 4, and their difference is within the standard deviations of the measurements for both castings.

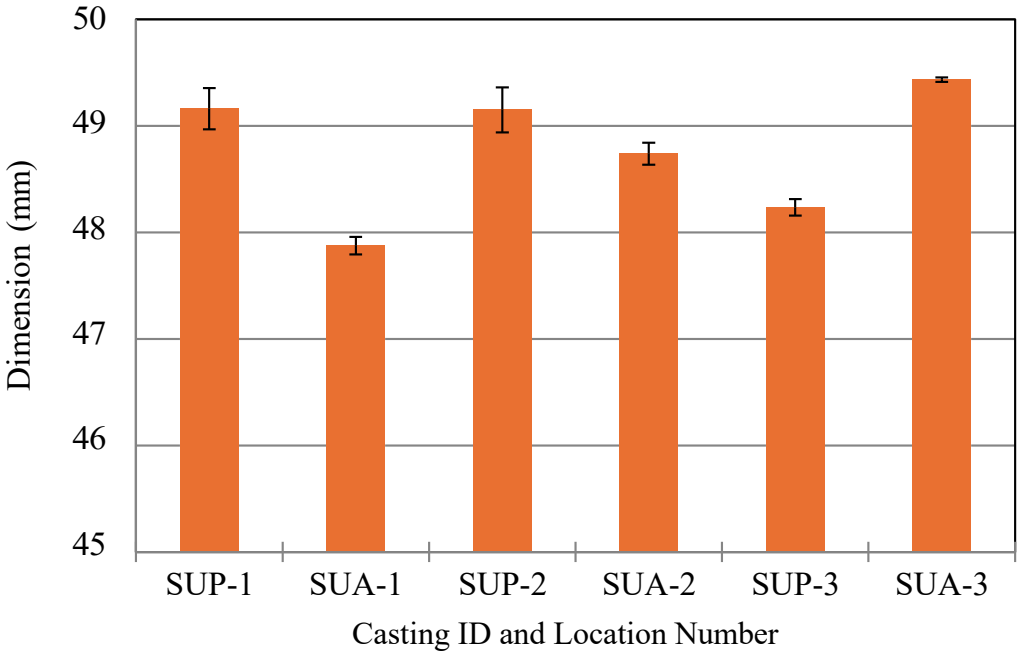

(a)

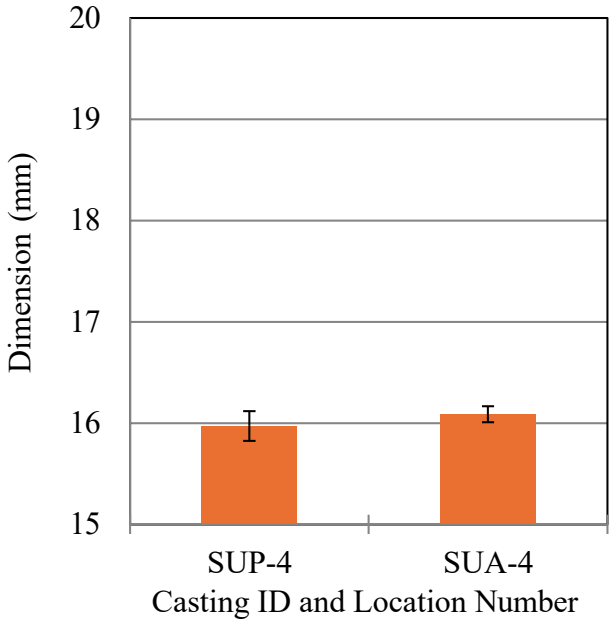

(b)

Figure 24 Average dimensions at the four locations for the pressurized and unpressurized castings are plotted with the error bars showing +/- one standard deviation of the five measurements. Locations 1, 2 and 3 are given in (a), and location 4 in (b).

The pressurized and unpressurized casting dimensions are compared next by plotting their differences. The differences in the dimensions (pressurized dimension – unpressurized dimension) are plotted in Figure 25. In the figure the error bars are the larger of the two standard deviations of the measured dimensions. The largest differences between the dimensions are at location 1 (nearest pressurized feeder) and location 3 (farthest from the pressurized feeder). At location 4 in the plot, the bill thickness, there is no discernable difference between the pressurized and un-pressurized dimension.

The application of pressure results in a significantly larger thickness of the ring nearest the feeder. The pressure seems prevent the usual solidification shrinkage of the casting surface. At location 2, the pressurized casting's ring thickness is only marginally larger and there is no significant difference. This location is at the hot spot. At location 3, furthest from the feeder, the dimension difference is opposite the observation at location 1. It might have been expected that the pressure had little effect at location 3 with little difference between the two castings. The difference at location 3 is noteworthy. There is no difference in the bill thickness at location 4 as mentioned above. The plot in Figure 25 makes this clear. Clearly pressure has little effect on the feeding of a rangy thin section like the bill. It was found to eliminate the gas porosity as seen in Figure 8.

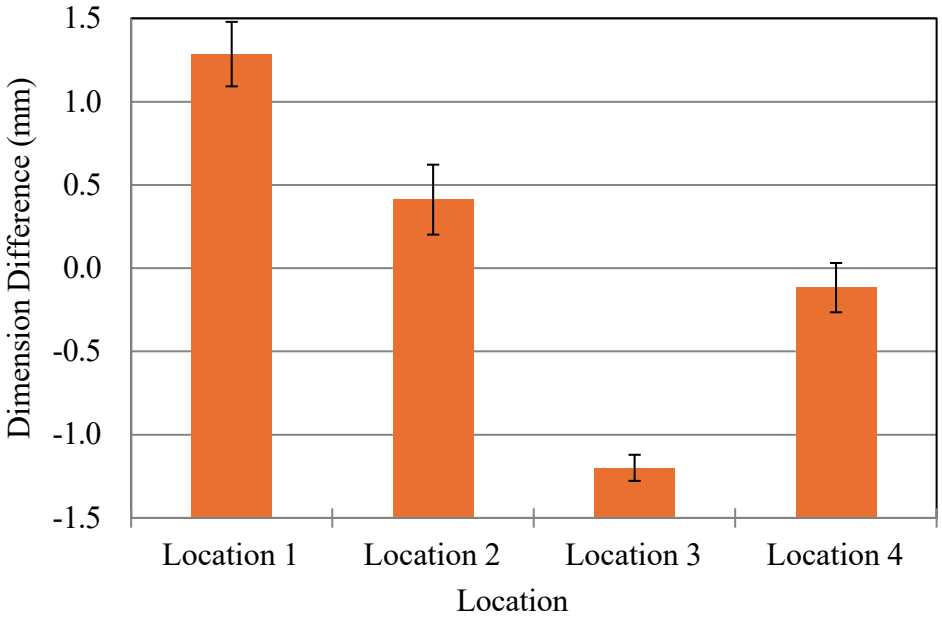

Figure 25 Comparison of differences in dimensions for platypus castings at locations 1 to 4. Difference plotted is (pressurized dimension – unpressurized dimension).

3.3 Tensile Properties of Pressurized and Unpressurized Castings

Tensile testing specimens were cut from the unpressurized and pressurized castings to investigate the effect of the pressure on mechanical properties. Twelve specimens were taken from each casting. The specimens were sectioned out of the castings after heat treatment. The mechanical/tensile property measurements were performed at an independent laboratory according to the ASTM E8-21 standard. The tensile data reported by the lab were yield strength (*YS*), ultimate strength (*UTS*), elongation (*EL*) and reduction of area (*RA*). The locations of the specimens and their identification characters are shown in Figure 26(a) to Figure 26(c). The specimens were identified as types "F" (two specimens), "H" (four specimens), and "V" (six specimens). As can be observed in Figure 26(b), several specimen sizes were used in this study having gage section diameters of 0.357 (specimen H4), 0.250 (specimen F2) and 0.505 inches (all other specimens).

The strength data results are shown in Figure 27. Yield strength is given in Figure 27(a) and ultimate strength in Figure 27(b). For specimen V6 the unpressurized casting's yield strength data was not reported. However, for that specimen, the ultimate strength was reported as plotted in Figure 27(b). The strengths results show no difference in either strength measure between the pressurized and unpressurized castings, except for specimen V6. Specimen V6 is near the hot pot location. For specimen V6 the pressurized casting ultimate strength is over 30 ksi higher than the unpressurized casting. It has been found in previous work that porosity (if that is what the pressure affects) has little or no effect on strength. A specimen with porosity can have a higher strength from tensile testing measurement than a specimen without porosity. Typically though, a specimen with porosity will have lower ductility.

The ductility data results are shown in Figure 28. In contrast to the relatively uniform strength data, the ductility data shows great variability with both the specimen locations and the pressurization of the castings. The elongation is plotted in Figure 28(a) by specimen ID and pressurization condition, and similarly the reduction of area is plotted in Figure 28(b). For the ductility, comparing pressurized and unpressurized castings, sometimes there is no difference between them, and sometimes one or the other has higher ductility. The specimens having approximately the same ductility regardless of pressurization condition are F2, H3, V1, V3, V4, and V5 (indicated by green circled IDs in Figure 29). The specimens having significantly greater ductility in the pressurized castings are H4, V2 and V6 (indicated by red circled IDs in Figure 29). The specimens having slightly greater ductility in the pressurized castings are H1 and H2 (indicated by dashed red circled IDs in Figure 29). The specimen having significantly greater ductility in the unpressurized casting is F1 (indicated by blue circled ID in Figure 29).

Focusing on specimen V6 first, its ductility for the unpressurized casting is the lowest of all specimens, and the pressurized casting has considerably greater ductility. It is among the most ductile specimens. As mentioned above this specimen is near the hot spot location. Specimen V2 has much higher ductility for the pressurized casting, and for the unpressurized casting the ductility is very low by comparison. This result is likely due to the applied pressure reducing the gas or inclusion/gas related indications seen in the radiographs of the unpressurized casting and images of its cope surface. The higher ductility at H4 for the pressurized casting is likely due to it being the closest specimen material to the pressurized feeder. Pressurization seems to have no effect on ductility for the green circled specimen IDs, and for the farthest specimen from the feeder F1

circled in blue. For specimen F1 the ductility was greater for the unpressurized casting. In this study, when the ductility is improved by pressurization, the improvement is most likely due to reduced gas porosity.

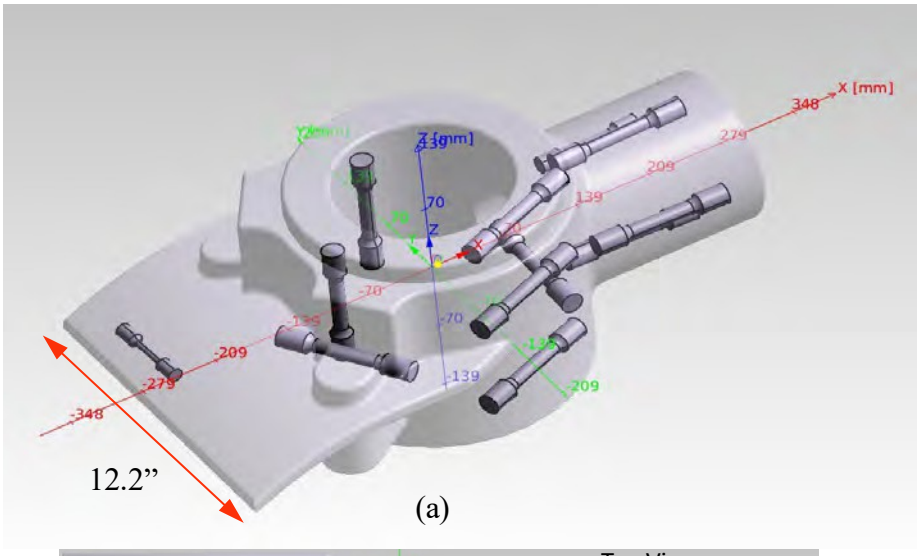

(a)

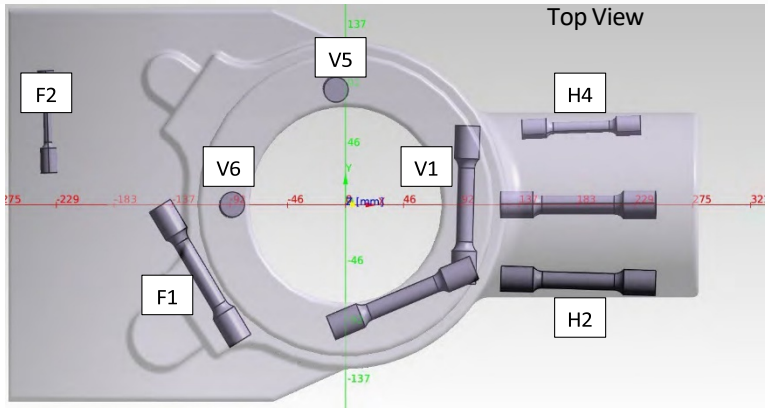

(b)

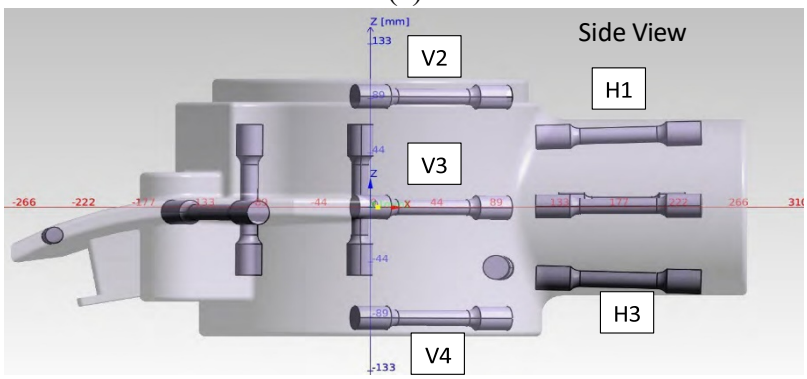

(c)

Figure 26 Views (a), (b), and (c) in an x-ray format of the locations of the twelve specimens sectioned out of the platypus castings after heat treatment for tensile testing.

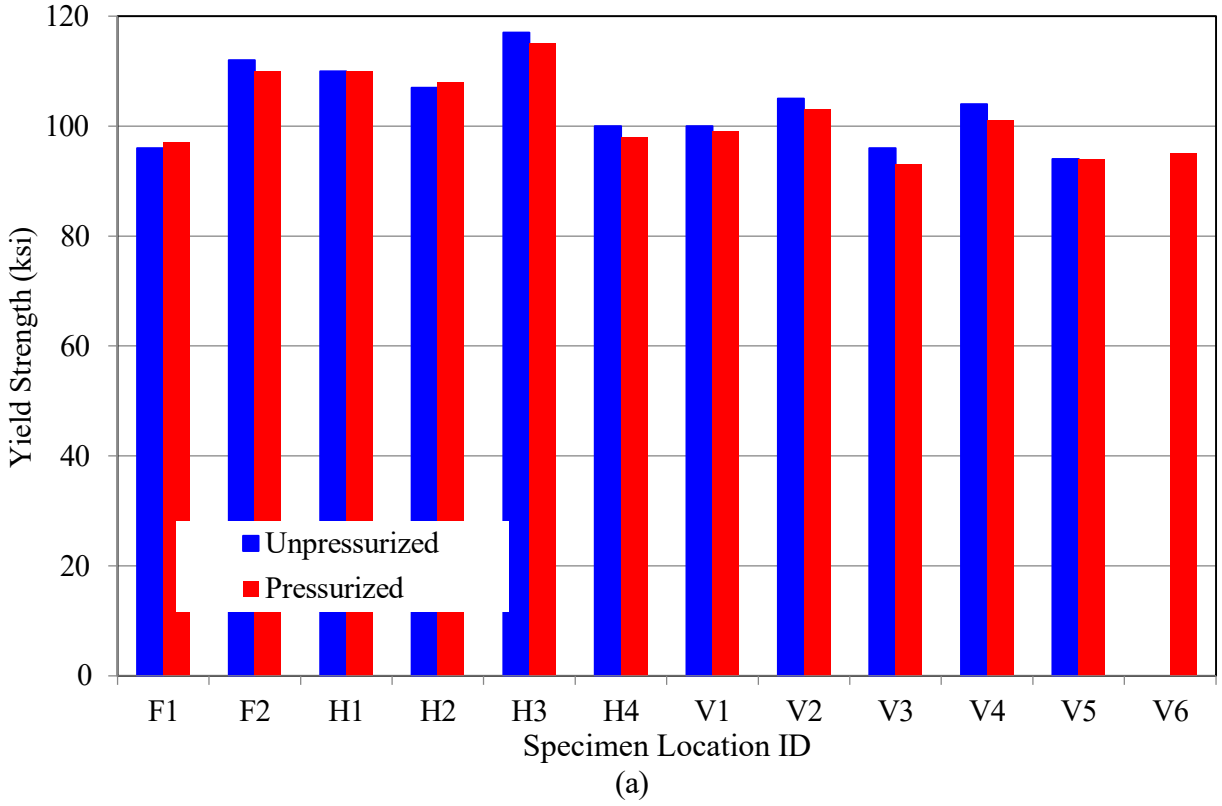

(a)

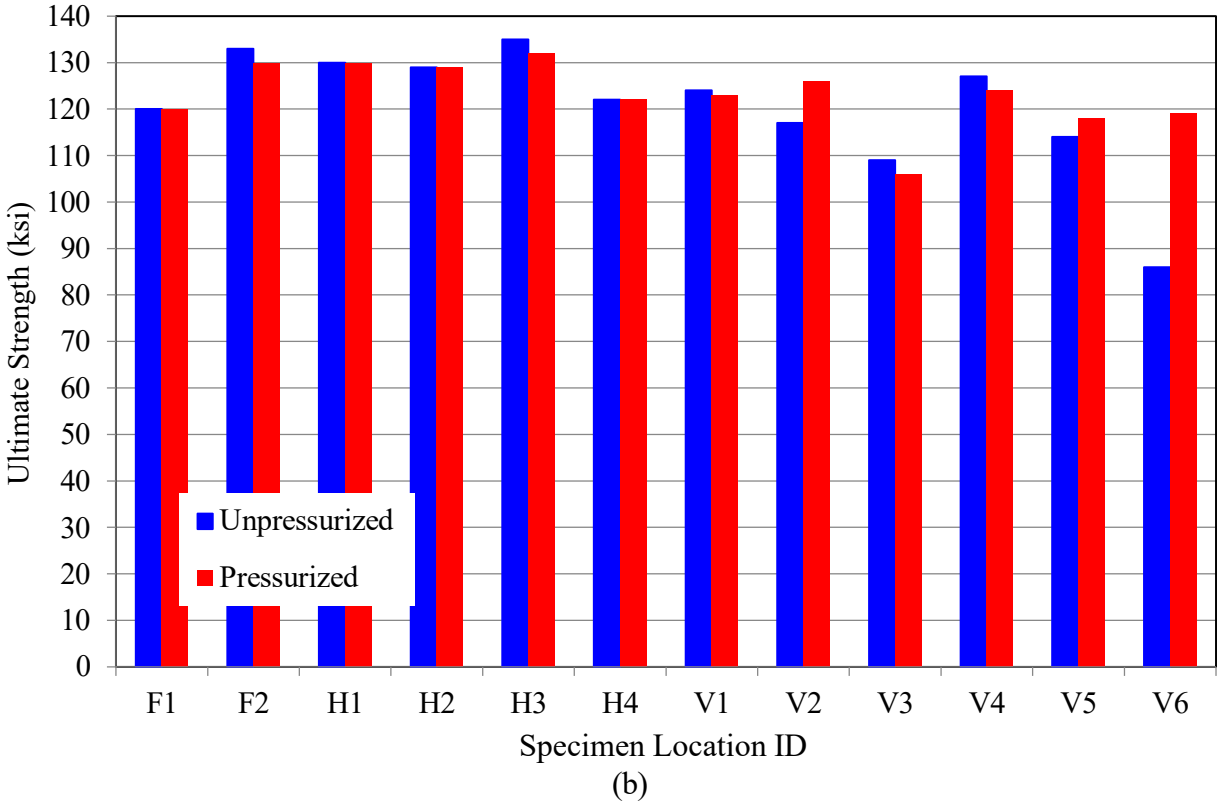

(b)

Figure 27 Strength data for unpressurized and pressurized castings (a) yield strength and (b) ultimate strength.

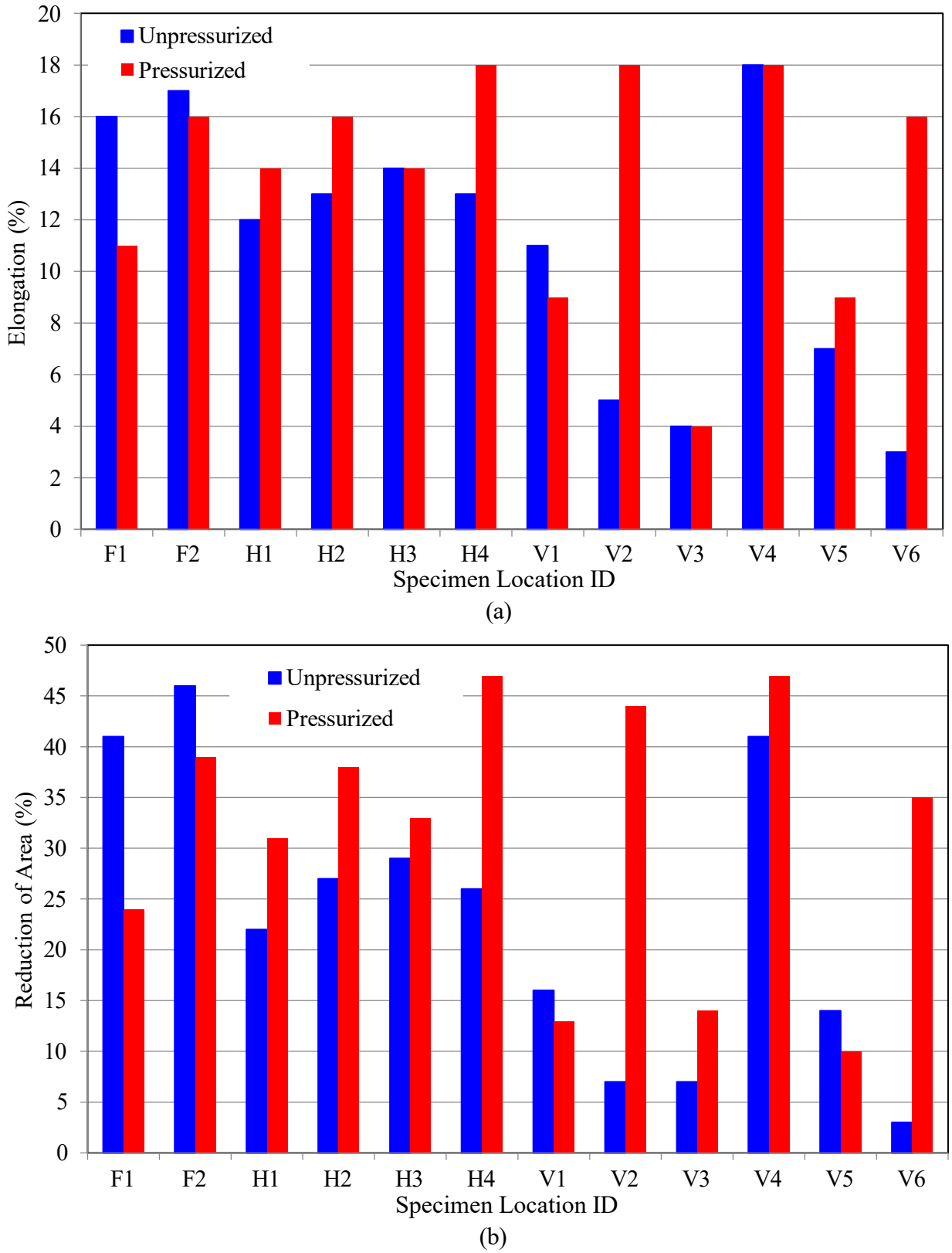

Figure 28 Ductility data for unpressurized and pressurized castings (a) elongation and (b) reduction of area.

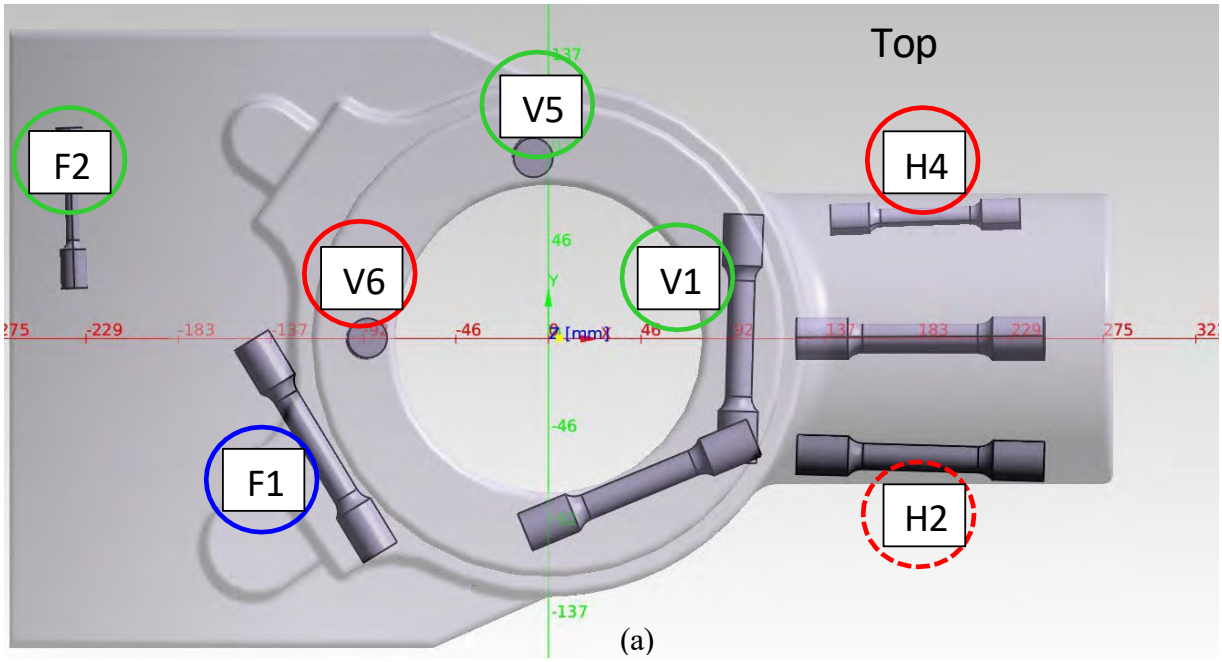

(a)

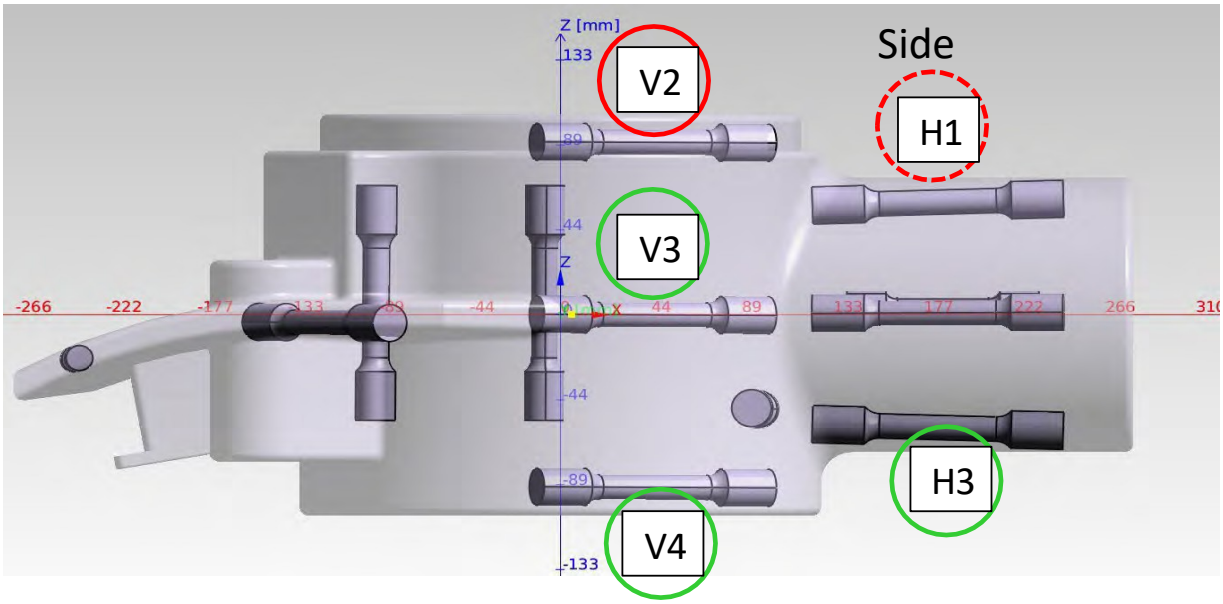

(b)

Figure 29 Top view (a) and side view (b) of specimens and their IDs with: 1) green circles indicating similar ductility in both pressure conditions, 2) red circles indicating pressurized casting had significantly greater ductility, red dashed circles indicating pressurized casting having marginally greater ductility, and blue circle indicating unpressurized casting having greater ductility.

The wedge showed minimal difference in UTS, elongation or max pore cluster size based on being pressurized or not (Figure 30). When pressurized, there was a small decrease in max pore, which resulted in the typical increase in ductility. With specimens taken at T/2, the difference in UTS is expected only to be a section size heat treatment effect with higher specimen location in the wedge, 7, having lower UTS than a lower location, 1.

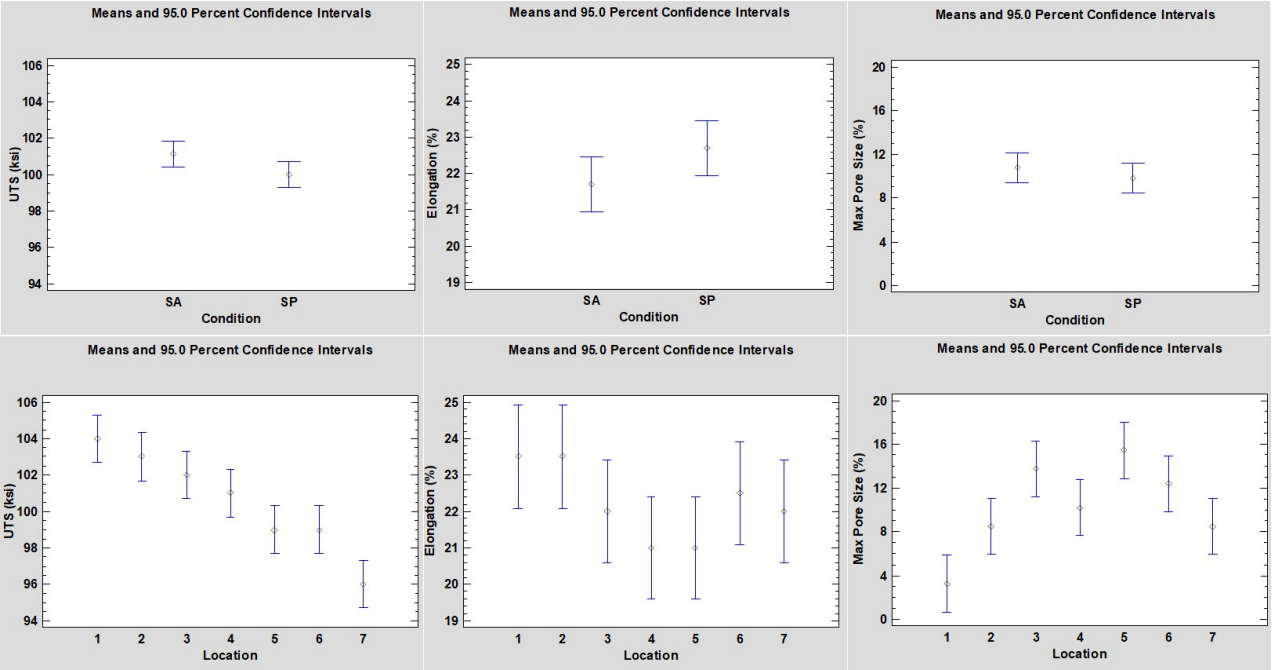

Figure 30: Wedge UTS, elongation and max pore cluster size

The plate castings were sectioned to remove three tensile coupons; the R, C, and D designations on the tensile ID are for Riser, Center, and Drag (Figure 31). As expected, there is little difference in tensile properties (Table 5) due to the ductile CF grade used and rigging the plate for good feeding. At the time of this paper, porosity fracture surface analysis was not yet completed nor any analysis to demonstrate pressurization in a nitrogen atmosphere increased cooling rate.

Figure 31: Plate specimen locations

Table 5: Plate mechanical properties

Sample ID	Alloy	UTS (ksi)	YTS (ksi)	Elongation (%)	RA (%)
SA-4-R	CF3	86	38.9	59	49
SA-4-C	CF3	88	39.9	56	50
SA-4-D	CF3	85	38.2	62	78
SA-6-R	CF3M	70	33.0	51	85
SA-6-C	CF3M	72	34.9	51	73
SA-6-D	CF3M	75	34.9	55	77
SP-4-R	CF3	86	38.7	60	59
SP-4-C	CF3	88	40.2	62	58
SP-4-D	CF3	85	39.5	53	67
SP-6-R	CF3M	72	31.6	63	83
SP-6-C	CF3M	72	32.5	55	79
SP-6-D	CF3M	73	32.4	61	81

3.4 Mechanical Testing Specimen Analysis

For the HS platypus, Figures 32 and 33 are from a multifactor ANOVA with two factors: location of the tensile in the casting and condition (SP and SA). This graph shows only the effect of condition; the effect of location is removed. Two conclusions:

1. Elongation increased by approximately 3% when solidified under pressure (SP) compared to an identical platypus casting solidified under unpressurized conditions (14% vs. 11%) (Figure 32).
2. Maximum pore size/tensile diameter ratio decreased from 32% to 17% when solidified under pressure (Figure 33).

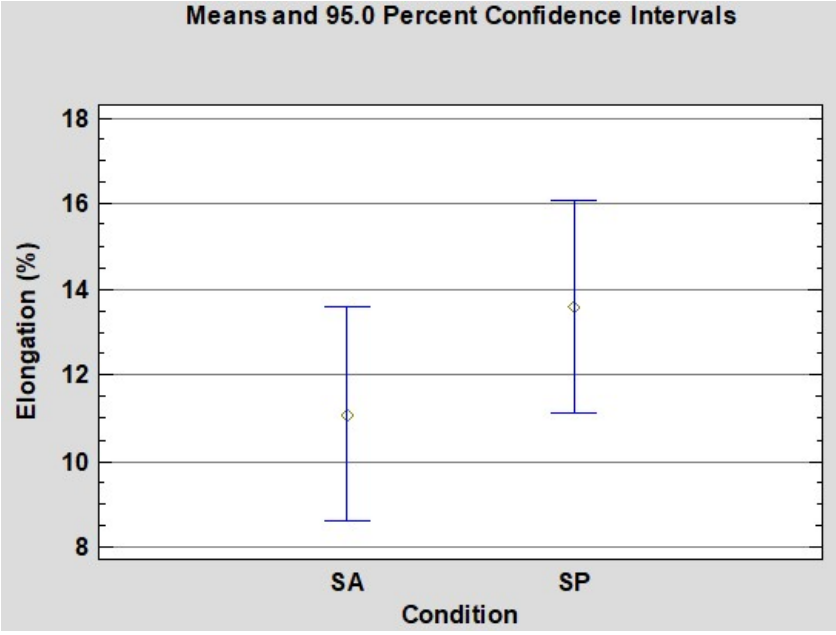

Figure 32: HS platypus elongation multifactor ANOVA analysis

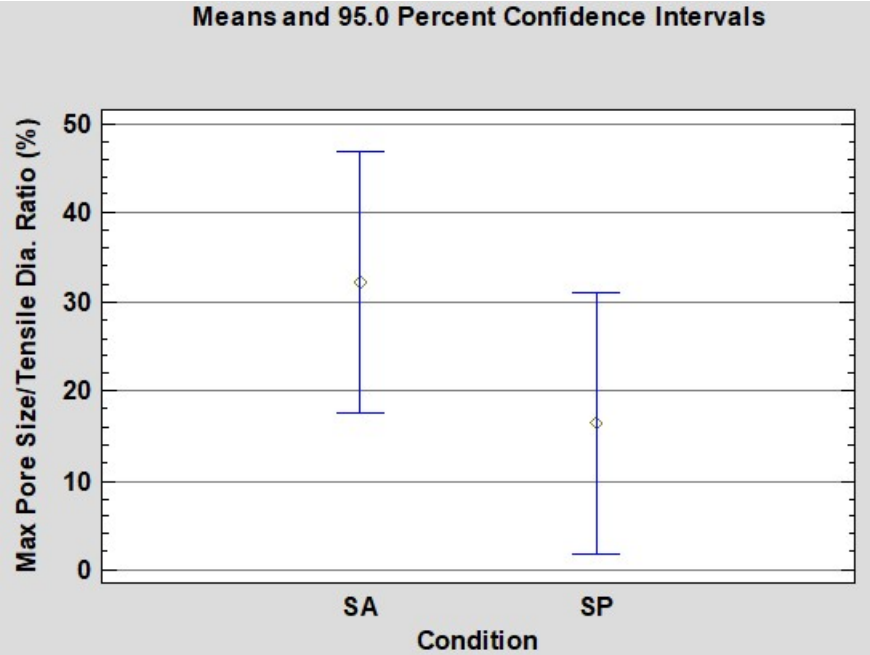

Figure 33: HS platypus max pore size/tensile diameter ratio multifactor ANOVA analysis

Of note, one specimen, SP-V3, in the pressurized platypus did have uncharacteristic large gas holes on the fracture surface (Figure 34). This was not observed on any of the other test specimens in this trial or any platypus trial.

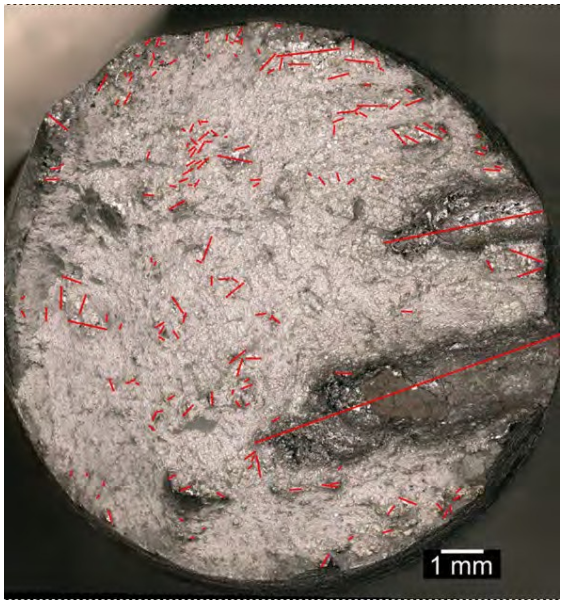

Figure 34: Large gas holes on fracture surface of test specimen

At the time of this paper, initial testing did not demonstrate faster solidification (e.g. grain size comparison). Unfortunately, thermocouple data was not successfully obtained during the trials.

4. Conclusions

A pressurized casting trial was performed where two sand castings were produced from 8630 steel, and one was placed in a sealed vessel and pressurized to 10 atmospheres. Both castings were filled through the riser. The fill time for the unpressurized casting was 12.6 seconds. The pouring time for the pressurized casting was 15 seconds. For the pressurized casting, pressurization began 51 seconds after the start of pouring. The maximum pressure applied was 10 atmospheres (150 psi) which was reached 125 seconds after the start of pouring. The pressure was applied for 25 minutes until the casting was solidified.

Radiographs were taken of the castings from 8 views. From the radiography it was observed that the benefit of the pressure was either preventing the formation of gas porosity or healing it after it formed. The pressure had little effect on feeding the hot spot in the casting. The porosity observed at that location appeared similar in both castings. The surface appearance of the pressurized casting was significantly improved from the unpressurized casting surface. This appeared to be related to gas porosity near the cope surface of the unpressurized casting.

Casting process simulations were performed using an advanced feeding porosity model that computes the pressure and feeding flow in the casting process. The model was run using environmental pressures of 1 and 10 atmospheres, just like the pressure vessel used in the trial. The model does not predict gas porosity. The model predicted lower microporosity in the pressurized casting. At the hot spot, the model predicted little difference in porosity for the castings. The model gave additional insight on the effect of pressure to extend the time of feeding flow through the solidifying section to the hot spot. For the pressurized casting, it was estimated that the feeding flow is cut off at 96% of the total casting system solidified. For the unpressurized casting the feeding flow from the riser was cut off at 94% solidified. Considering the times to these points in the solidification process, the application of pressure was predicted to provide an additional 77 seconds of feeding flow from the feeder to the hot spot.

Section thickness dimension measurements were made at four locations in the pressurized and unpressurized castings. For two of the locations, at the hot spot and the thin bill section (16 mm or 0.63” thick), no appreciable difference was found in the measurements. At the other two locations there were significant differences in the dimensions of the pressurized and unpressurized thickness dimensions. At the location near to the feeder, the pressurized casting thickness was significantly larger than the unpressurized casting thickness. Then at a location farther from the feeder the opposite behavior was observed, and the unpressurized casting thickness was larger than the pressurized casting thickness.

Twelve tensile specimens were taken from both castings in the pressurization trial at matching locations. Only one of the specimen locations showed differences in strength between the unpressurized and pressurized castings. For that location, near the hot spot, the pressurized casting specimen had higher strength. For the ductility measurements, comparing pressurized and unpressurized castings, at six of the locations no difference in ductility was observed between the two castings. At three locations the pressurized casting has significantly greater ductility. At two locations the pressurized casting had marginally greater ductility. At one specimen location the unpressurized casting had significantly larger ductility than the pressurized casting. The improved ductility observed in the pressurized casting specimens is likely the result of reduced gas porosity

observed comparing the unpressurized and pressurized castings' radiography results.

For future pressurized casting trials, simpler casting geometries should be used to understand the fundamental effects and benefits of pressurization on the steel casting process. For example, a long plate or bar could be used to demonstrate how pressurization can eliminate centerline shrinkage and extend feeding distances. Also, the benefits of pressurization applied to rangy castings, blind feeders and feeding long vertical sections should be investigated. The timing to pour and close the vessel likely means a skin will form before pressurization, and the pressure is too low to act like a HIP effect. However, if hot topping is utilized, it will promote the feeder being able to be acted on by the increased pressure. Finally, thermocouple data should be acquired to assess if pressure and a nitrogen can provide improved heat transfer or if the enclosed environment of the vessel limits this by not allowing heat to readily escape.

Acknowledgment: Research sponsored by the DLA Troop Support, Philadelphia, PA and the Defense Logistics Agency Information Operations, J68, Research & Development Office, Ft. Belvoir, VA

Acknowledgements

This work would not have been possible without the help and support from Harrison Steel (especially Shawn Martin and Jacob Melvin), Waukesha Foundry (especially Steve Cooke and Alex Kerwin) and Foundry Casting Systems (especially Charlie Murray).

References

[1] Hardin, R., Hays, T., and Beckermann, C., "Pressurized Riser Casting Trials," in *Proceedings of the 55th SFSA Technical and Operating Conference*, Paper No. 3.8, Steel Founders' Society of America, Chicago, IL, 2001.

[2] Archer, L., Hardin, R., and Beckermann, C., "Counter Gravity Sand Casting of Steel with Pressurization During Solidification," in Proceedings of the 71st SFSA Technical and Operating Conference, Paper No. 3.7, Steel Founders' Society of America, Chicago, IL, 2017.

[3] Bryant, N., Thiel, G., Foley, R., and Griffin, J., "Pressurized Solidification of Steel Castings," in Proceedings of the 77th SFSA Technical and Operating Conference, Paper No. 5.6, Steel Founders' Society of America, Chicago, IL, 2023.

[4] Hardin, R., and Beckermann, C., "Effect of Cooling Rate and Microporosity on Mechanical Performance of a High Strength Steel," in Proceedings of the 70th SFSA Technical and Operating Conference, Paper No. 5.2, Steel Founders' Society of America, Chicago, IL, 2016.

[5] Navsea Technical Publication T9074-BD-GIB-010/0300 Rev. 2, "Base Materials for Critical Applications: Requirements for Low Alloy Steel Plate, Forgings, Castings, Shapes, Bars, and

Heads of HY-80/100/130 and HSLA-80/100,” Appendix D, 2012.

[6] Hardin, R., and Beckermann, C., "Mechanical Properties of Commercial 8630 Q&T Steel Castings: Testing Results Compared to Simulations," in Proceedings of the 76th SFSA Technical and Operating Conference, Paper No. 4.1, Steel Founders' Society of America, Chicago, IL, 2022.

[7] Khalajzadeh, V., and Beckermann, C., "Advanced Modeling of Shrinkage Porosity and Application to Mn-Steel Castings," in Proceedings of the 72nd SFSA Technical and Operating Conference, Paper No. 5.7, Steel Founders' Society of America, Chicago, IL, 2018.

[8] Khalajzadeh, V., and Beckermann, C., "Simulation of Shrinkage Porosity Formation During Alloy Solidification," Metall. Mater. Trans. A, Vol. 51A, 2020, pp. 2239-2254.